Structural and Multidisciplinary Optimization (2022) 65:34
https://doi.org/10.1007/s00158-021-03118-4

RESEARCH PAPER

# Topology optimization of turbulent fluid flow via the TOBS method and a geometry trimming procedure

**Renato Picelli[1] · Eduardo Moscatelli[2] · Paulo Vinícius Miyuki Yamabe[2] · Diego Hayashi Alonso[2] · Shahin Ranjbarzadeh[2] · Rafael dos Santos Gioria[1] · Julio Romano Meneghini[3] · Emílio Carlos Nelli Silva[2]**

Received: 23 February 2021 / Revised: 20 October 2021 / Accepted: 15 November 2021 / Published online: 6 January 2022


**Abstract**
One of the current challenges for topology optimization methods is the consideration of high Reynolds fluid flow analysis, especially including turbulence models. The issues in current pseudo-density-based methods are threefold. The fluid boundaries are unknown during optimization, the convergence to $\{0, 1\}$ designs might be highly dependent on the tuning of the optimization parameters and it is difficult to specify the maximum value of the inverse permeability to avoid the presence of fluid flowing inside the modeled solid medium. This paper proposes a methodology to tackle these three problems. The Topology Optimization of Binary Structures (TOBS) method and a geometry trimming procedure are employed to create the TOBS-GT method. This method uses a binary $\{0, 1\}$ design variable, which naturally creates explicit fluid boundaries during optimization and avoids the need for tuning the material model interpolation parameters. The geometry trimming procedure removes the solid regions and create a CAD model with only the fluid analysis domain and smooth walls. Since there is no solid region inside the analysis mesh, the problem of having fluid flowing through a solid region is avoided. The $k$-$\varepsilon$ and $k$-$\omega$ turbulence models are chosen to illustrate that the method may be applied to any turbulence model. The equilibrium equations are solved using the finite element method. The total fluid energy dissipation is minimized considering a fluid volume constraint. Numerical results show that the TOBS-GT method is well-fitted for topology optimization of turbulent fluid flow problems.

**Keywords** Fluid flow topology optimization · Turbulent flow · Turbulence · TOBS · Integer linear programming · Finite Element Method

## 1 Introduction

Topology optimization (TO) is a computational engineering tool used to provide optimized geometries, with highly attractive applications in the areas of structural and fluid flow path designs. The main goal of TO is to solve a material distribution problem within the design domain considering an objective function and a set of possible constraints. In the case of fluids, the design variables $\{1\}$ and $\{0\}$ usually indicate regions of the domain where the fluid is free to flow ("fluid") and restricted to flow ("solid"), respectively. However, current TO methods usually relax the binary variable $\{0, 1\}$, which occasionally leads to grayscale regions, with intermediate properties between fluid and solid. That is not an issue for some problems; however, it is an essential aspect of fluid dynamics since the contour in a fluid mesh must be modelled with caution, especially in high Reynolds flows.

The use of the TO method for fluid problems began with the seminal work of Borrvall and Petersson (2003). The authors proposed to minimize the fluid energy dissipation in 2D channels, subject to a volume constraint using the incompressible Stokes flow equations and adding the Brinkman penalization on the design variables.

Responsible Editor: Julián Andrés Norato

✉ Renato Picelli
rpicelli@usp.br

[1] Department of Mining and Petroleum Engineering, Polytechnic School of the University of São Paulo, São Paulo, SP, Brazil

[2] Department of Mechatronics and Mechanical Systems Engineering, Polytechnic School of the University of São Paulo, São Paulo, SP, Brazil

[3] Department of Mechanical Engineering, Polytechnic School of the University of São Paulo, São Paulo, SP, Brazil

Gersborg-Hansen et al. (2006) extended the work in Borrvall and Petersson (2003) by optimizing the flow for a wider range of Reynolds numbers considering inertial fluid effects and nonlinearities, i.e., using the incompressible Navier-Stokes (N-S) equations. After these advances, interesting applications were achieved, e.g., the design of fluid devices in valves (Song et al. 2009), mixers (Andreasen et al. 2009), rectifiers (Jensen et al. 2012) and flow machine rotors (Romero and Silva 2014). Sá et al. (2018) performs the complete development cycle of a small-scale pump designed using the TO method. The 2D swirl flow model is applied in TO to reduce the computational cost for designing 2D swirl flow devices in relation to using a complete 3D model (Alonso et al. 2018). Pingen and Maute (2010) and Hyun et al. (2014) considered non-Newtonian fluid effects in the systematic design of fluidic systems dealing with blood. All these works show the outstanding capabilities of TO when designing innovative fluid devices at low-speed flow. On the other hand, when it comes to higher levels of complexity of fluid flow, such as larger and higher speed fluid flow systems, TO's current methodologies are still not sufficiently developed. In practice, these are the targets of many engineering applications, such as in the aerospace, automotive, and oil and gas industries, to cite a few. For these problems, the works mentioned above cannot incorporate well or cannot incorporate fluid model's complexity at all.

One of the current most challenging applications of TO methods for fluid flow design includes the consideration of turbulence (Alexandersen and Andreasen 2020). Othmer (2008) pointed up the first research direction for turbulent flow TO by exploring sensitivity maps via the continuous adjoint approach. However, the "frozen turbulence" assumption was adopted, in which the variation in the turbulent viscosity with respect to the design variables is neglected. Later on, Kontoleontos et al. (2013) presented an exact continuous adjoint formulation for TO, that takes into consideration the differentiation of the low-Reynolds number Spalart-Allmaras model. The challenges rapidly showed to be the modelling of the turbulence and the computations of its sensitivities. Papoutsis-Kiachagias and Giannakoglou (2016) and Yoon (2016) developed the complete TO frameworks for turbulent flows using the Spalart-Allmaras model by considering the sensitivity related to the wall distance computation. Dilgen et al. (2018a) used the Spalart-Allmaras and $k$-$\omega$ models for performing TO for turbulent flows, also exploring the benefits of automatic differentiation. The same research group applied the method to heat sink design with turbulent forced convection (Dilgen et al. 2018b). More recently, Yoon (2020) modified the $k$-$\varepsilon$ turbulence model to carry out TO and Sá et al. (2021) introduced a rotation correction for the turbulence evaluation when rotating frames are considered using the Spalart-Allmaras model. Lee et al. (2020) explored the use of simplified sensitivities by neglecting the exact adjoint analysis, for an aero-thermal system.

All of these previous works are based on the continuous pseudo-density distribution within the fluid design domain and attempt to improve the turbulence modelling and sensitivity calculation in the TO framework. A material interpolation model (e.g. SIMP, RAMP or the model proposed by Borrvall and Petersson (2003)) is required to allow for continuous pseudo-density changes. An inverse permeability term is employed in the attempt of restricting the fluid not to flow inside the modeled solid regions. In this context, one can point out three issues. First, intermediate pseudo-densities create a large amount of grayscale, leading the fluid domain walls not to be explicitly defined due to the continuous transition between the fluid and solid regions. This is numerically not recommended in some fluid dynamics problems and represents a considerable obstacle when dealing with fluid flows that require mesh refinement or specific boundary conditions at walls – e.g. turbulence wall functions. Second, the material interpolation model leads the numerical analysis to be highly dependent on a penalization factor. Frequently, the tuning of the penalization parameters during optimization is non-intuitive and should be changed dynamically in order to push intermediate pseudo-density values to the $\{0, 1\}$ bounds. Third, the value of the inverse permeability may be difficult to be determined and may be case-dependent. These three issues preclude the pseudo-density-based TO method to account for more rigorous numerical analysis, including turbulence models with wall functions. Even when the design successfully converges to $\{0, 1\}$ topologies, the fluid velocity is dropped towards zero when going from 1 (fluid) to the interfaces, by decreasing the solid material permeability, but no actual wall function or boundary condition is applied. These issues motivate the development of TO methods that do not rely on intermediate pseudo-densities, such as the level-set (Feppon et al. 2019) and binary approaches (Souza et al. 2021). Recently, Kubo et al. (2021) developed a level set framework for turbulent flow TO with wall functions, but assuming frozen turbulence.

This work's main objective is to propose a TO methodology that tackles the three aforementioned problems while considering its application to turbulent flow TO. The Topology Optimization of Binary Structures (TOBS) method is a fair candidate for such a case (Sivapuram and Picelli 2018). The method employs binary $\{0, 1\}$ design variables. This feature produces explicitly defined fluid boundaries during optimization, which allows the direct application of turbulent wall functions and other relevant conditions. Also, the effects of penalizing intermediate pseudo-density values are naturally avoided since no intermediate pseudo-densities are present. The TOBS method generalizes the binary TO problem by using sequential

integer linear approximation and move limits. The method differs from other binary approaches by the use of Integer Linear Programming (ILP) (Paul 2009). Herein, the Finite Element Analysis (FEA) is used to solve the Reynolds-Averaged Navier-Stokes (RANS) equations. The total fluid energy dissipation (considering the viscous and turbulent effects) is minimized subject to a volume constraint. The governing equations and adjoint sensitivities are solved Via COMSOL Multiphysics® fluid dynamics and automatic differentiation modules. Souza et al. (2021) first applied the TOBS method to fluid flow optimization using the standard inverse permeability approach. Herein, the use of a geometry trimming procedure is proposed in order to remove the modeled solid regions from the analysis, consequently eliminating the inverse permeability term. The inverse permeability is still used to aid the sensitivity analysis but with no actual effect in the final topology solution due to the absence of a modeled solid region. Furthermore, the permeability term is modeled with a linear interpolation scheme. The geometry trimming approach has been idealized for fluid-structure interaction problems by (Picelli et al. 2020a) but herein formalized. First, a set of optimization grid points is defined as design domain by a regular structured mesh. The countours of the $\{0,1\}$ designs produced by TOBS are extracted and smoothed. A CAD (computer-aided design) model is produced by trimming the solid regions (where the variable is $\{0\}$) out of the initial full geometry. The remaining geometry is left to be automatically meshed by the finite element software based on the physics to be solved. A brief illustration of the method is given in Fig. 1. Herein, the TOBS method added with the geometry trimming step is so called TOBS-GT. The trimming process automatically generates walls for the fluid flow that can be directly treated according to the fluid flow requirements. Herein, the $k$-$\varepsilon$ or $k$-$\omega$ turbulence wall functions are employed. Besides, freely generated meshing can also offer benefits when refining the mesh in appropriate regions, e.g., near walls and geometric features. In fact, the TOBS-GT method aims to allow the digital $\{0,1\}$ framework to accommodate convenient tools from CAD modelling and Computational Fluid Dynamics simulation via its surface-capturing approach. To the authors' best knowledge, this is the first work to solve turbulent fluid flow TO imposing explicit turbulence wall functions without the frozen turbulence assumption. Other contributions include the use of an ILP solver and the solution for three-dimensional problems. The main novelties of this work are the following:

- A new surface-capturing method (TOBS-GT) is created for topology optimization by combining binary design variables, smooth contour extraction and geometry trimming;
- The proposed method may be independent of the penalization for the pure fluid optimization problem;
- The proposed TOBS-GT designs tend to look like solutions of standard fluid flow topology optimization but with no need to select the inverse permeability values nor penalization parameters.
- Topology optimization of turbulent fluid flow problems is carried out imposing turbulence wall functions;

The remainder of the paper is organized as follows. In Sect. 2, the governing equations for the turbulent fluid flow modelling are presented. In Sect. 3, the formulation of the topology optimization method is presented alongside the TOBS algorithm. In Sect. 4, the geometry trimming procedure is detailed and the TOBS-GT method is formalized. In Sect. 5, two-dimensional (2D) and three-dimensional (3D) numerical examples are presented. In Sect. 6, some conclusions are inferred.

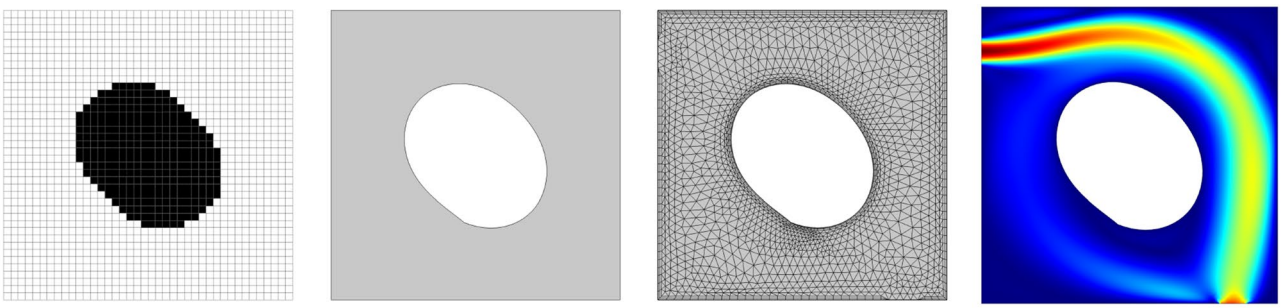

(a) $\{0,1\}$ design defined in a regular structured mesh. (b) Smoothed CAD extraction via geometry trimming. (c) Freely generated mesh by the FEA software. (d) Result of the FEA for the studied physics.

**Fig. 1** Illustration of the FEA set up produced by the TOBS-GT method

## 2 Governing equations

### 2.1 RANS equations

The turbulent motion of a fluid particle inside a fluid flow domain $\Omega_f$ (see Fig. 2) can be described by the RANS equations (Wilcox 1998; Larsson 1998) and can be solved by the Finite Element Method. Assuming a steady-state, homogeneous, isothermal, incompressible and Newtonian fluid flow without body forces, the RANS equations can be written as

$$\rho_f(\boldsymbol{v}\cdot\nabla\boldsymbol{v}) = \nabla\cdot\left[-p\boldsymbol{I}+\boldsymbol{\tau}_f\right]+\kappa(\alpha)\boldsymbol{v} \qquad \text{in } \Omega_f, \tag{1}$$

$$\nabla\cdot\boldsymbol{v} = 0 \qquad \text{in } \Omega_f, \tag{2}$$

where $\rho_f$ is the fluid density, $\boldsymbol{v}$ is the statistical time-averaged velocity, $p$ is the statistical time-averaged pressure, $\kappa(\alpha)$ is the inverse permeability (used in topology optimization, being described in Sect. 2.2), $\boldsymbol{I}$ is the identity matrix, and $\boldsymbol{\tau}_f$ is the shear stress tensor that includes the viscous and turbulent effects over the fluid, which is given by

$$\begin{aligned}\boldsymbol{\tau}_f &= 2\big(\mu+\mu_T\big)\boldsymbol{\epsilon}(\boldsymbol{v}),\\ \boldsymbol{\epsilon}(\boldsymbol{v}) &= \frac{1}{2}\big(\nabla\boldsymbol{v}+(\nabla\boldsymbol{v})^T\big),\end{aligned} \tag{3}$$

where $\mu$ is the fluid dynamic viscosity and $\mu_T$ is the isotropic eddy viscosity calculated with a turbulence model. The friction force term $\kappa(\alpha)\boldsymbol{v}$ is added in Eq. (1) in a similar fashion as in standard pseudo-density-based methods. However, when using the geometry trimming procedure, this term only influences the sensitivity, with no effects in the analysis (simulation), because the pseudo-density is binary, with the solid material being trimmed out of the analysis mesh. This is further explained in Sect. 2.2.equations can be written as

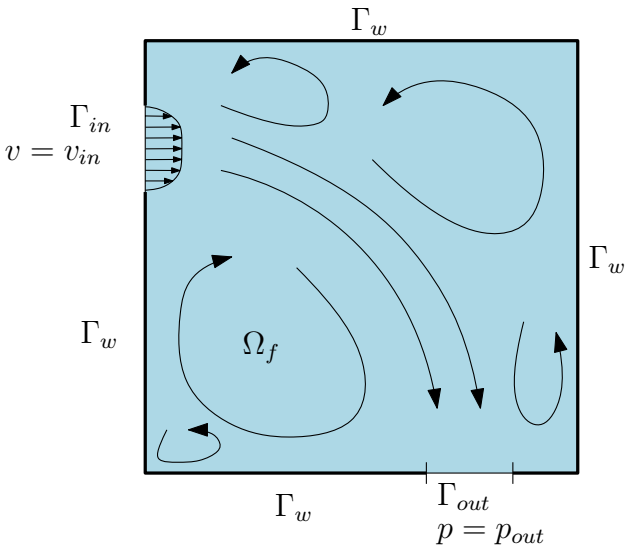


**Fig. 2** Illustration of the turbulent fluid flow problem. The fluid flows from an inlet boundary $\Gamma_{in}$ through a domain $\Omega_f$ bounded by the walls $\Gamma_w$ and exiting at an outlet boundary $\Gamma_{out}$

In contrast to laminar flow, the isotropic eddy viscosity $\mu_T$ is present in order to account for the normal and shear stresses caused by turbulent eddies on the fluid. The calculation of $\mu_T$ depends on the engineering application. Several approximation theories have been developed depending on the physical interpretation of the eddy viscosity models, each one presenting specific numerical limitations. These theories can also be referred as turbulence models. The $k$-$\varepsilon$ and $k$-$\omega$ models are common choices for a wide range of turbulence problems, and are used in this paper to illustrate that the proposed optimization procedure should work regardless the adopted model.

#### 2.1.1 *k*-$\varepsilon$ turbulence model

The inclusion of the turbulent effects via the standard $k$-$\varepsilon$ model is based on the transport of two additional turbulent quantities, namely the turbulent kinetic energy $k$ and its dissipation rate $\varepsilon$ (Wilcox 1998). In steady-state, these two additional balance equations can be written as

$$\rho_f\boldsymbol{v}\cdot\nabla k = \nabla\cdot\left(\left(\mu+\frac{\mu_T}{C_k}\right)\nabla k\right)+P_k-\rho_f\varepsilon+\kappa(\alpha)k, \tag{4}$$

$$\begin{aligned}\rho_f\boldsymbol{v}\cdot\nabla\varepsilon =& \nabla\cdot\left(\left(\mu+\frac{\mu_T}{C_\varepsilon}\right)\nabla\varepsilon\right)+C_{\varepsilon1}\frac{\varepsilon}{k}P_k\\ &-C_{\varepsilon2}\rho_f\frac{\varepsilon^2}{k}+\kappa(\alpha)\varepsilon,\end{aligned} \tag{5}$$

where $\mu$ and $\mu_T$ account for the molecular and turbulent effects of the viscosity, respectively, and the latter is defined in terms of the two additional turbulent fields

$$\mu_T = \rho_f C_\mu\frac{k^2}{\varepsilon}. \tag{6}$$

The material model terms $\kappa(\alpha)k$ and $\kappa(\alpha)\varepsilon$ are added to Eqs. (4) and (5), respectively, in order to obtain the derivatives with respect to the $k$-$\varepsilon$ turbulence variables. This approach is based on the work performed by Yoon (2020). The source terms in Eqs. (4) and (5) are written as a function of $P_k$, defined as

$$P_k = \mu_T\big(\nabla\boldsymbol{v}:\big(\nabla\boldsymbol{v}+(\nabla\boldsymbol{v})^T\big)\big). \tag{7}$$

The $k$-$\varepsilon$ model has five constants: $C_\mu = 0.09$, $C_{\varepsilon1} = 1.44$, $C_{\varepsilon2} = 1.92$, $C_k = 1.0$, and $C_\varepsilon = 1.3$.

The wall functions are such that the computational domain is assumed to be located a distance $\delta_w$ from the wall

(COMSOL 2019). The distance $\delta_w$ is automatically computed so that

$$\delta_w^+ = \frac{\rho_f v_\tau \delta_w}{\mu} = 11.06, \tag{8}$$

where $v_\tau = C_\mu^{1/4}\sqrt{k}$ is the friction velocity. The corresponding wall boundary conditions for the velocity are: a no-penetration condition $\boldsymbol{v}\cdot\boldsymbol{n} = 0$ and a shear stress condition given as

$$\boldsymbol{\tau}_f\cdot\boldsymbol{n} - \left(\boldsymbol{n}\cdot\boldsymbol{\tau}_f\cdot\boldsymbol{n}\right)\boldsymbol{n} = -\rho_f v_\tau \frac{\boldsymbol{v}}{v^+}, \tag{9}$$

where

$$v_\tau = \max\left(\frac{|\boldsymbol{v}|}{\frac{1}{\kappa_V}\ln\delta_w^+ + B}, C_\mu^{1/4}\sqrt{k}\right), \tag{10}$$

being $\kappa_V$ the von Kárman constant and $B$ a constant equal to 5.2 (COMSOL 2019).

#### 2.1.2 *k-ω* turbulence model

The revised $k$-$\omega$ model (Wilcox 2008) calculates the turbulent eddy viscosity $\mu_T$ as

$$\mu_T = \rho_f \frac{k}{\omega}, \tag{11}$$

where $\omega$ is the specific dissipation rate in this model. Similarly to the $k$-$\varepsilon$ model, two additional equations are solved to obtain the $k$-$\omega$ quantities (Wilcox 1998). They are:

$$\rho_f \boldsymbol{v}\cdot\nabla k = P_k - \rho_f\beta^* k\omega + \nabla\cdot\left(\left(\mu + \sigma^*\mu_T\right)\nabla k\right) + \kappa(\alpha)k, \tag{12}$$

$$\rho_f \boldsymbol{v}\cdot\nabla\omega = \alpha_T\frac{\omega}{k}P_k - \rho_f\beta_T\omega^2 + \nabla\cdot\left(\left(\mu + \sigma\mu_T\right)\nabla\omega\right) + \kappa(\alpha)\omega, \tag{13}$$

where $\beta_T = \beta_0 f_\beta$, $f_\beta = \frac{1+70\mathcal{X}_\omega}{1+80\mathcal{X}_\omega}$, $\mathcal{X}_\omega = \frac{\Omega_{ij}\Omega_{jk}\sigma_{ki}}{(\beta_0^*\omega)^3}$, $\beta^* = \beta_0^* f_{\beta^*}$, where

$$f_{\beta^*} = \begin{cases} 1 & \mathcal{X}_k \le 0 \\ \frac{1+680\mathcal{X}_k^2}{1+400\mathcal{X}_k^2} & \mathcal{X}_k > 0 \end{cases}, \tag{14}$$

with $\mathcal{X}_k = \frac{1}{\omega^3}(\nabla k\cdot\nabla\omega)$, being $\Omega_{ij} = \frac{1}{2}\left(\frac{\partial v_i}{\partial x_j} - \frac{\partial v_j}{\partial x_i}\right)$ the mean rotation-rate tensor and $\sigma_{ki} = \frac{1}{2}\left(\frac{\partial v_k}{\partial x_i} + \frac{\partial v_i}{\partial x_k}\right)$ the strain-rate tensor. The closure constants are $\alpha_T = 0.52$, $\beta_0 = 0.104$, $\beta_0^* = 0.09$, $\sigma = 0.5$, and $\sigma^* = 0.5$. The material model terms $\kappa(\alpha)k$ and $\kappa(\alpha)\omega$ are added to Eqs. (12) and (13), respectively, in order to obtain the derivatives with respect to the $k$-$\omega$ turbulence variables. This approach is based on the work of Dilgen et al. (2018a). Wall boundaries are treated with the same type of boundary conditions as for the $k$-$\varepsilon$ model with $C_\mu$ replaced by $\beta_0^*$. It can be pointed out that because of the geometry trimming, the material models for all equations can be identical.

#### 2.1.3 Boundary conditions

In order to solve the RANS equations, the following boundary conditions are applied:

$$\boldsymbol{v} = \boldsymbol{v}_0\left(\Gamma_{xyz}, v_{\text{in,ave}}\right) \qquad \text{on } \Gamma_{\text{in}}, \tag{15}$$

$$\boldsymbol{n}^T\left[-p\boldsymbol{I} + \boldsymbol{\tau}_f\right]\boldsymbol{n} = -\hat{p}_0 \qquad \text{on } \Gamma_{\text{out}}, \tag{16}$$

$$\hat{p}_0 \le p_{\text{out}}. \tag{17}$$

Eq. (15) represents the velocity profile given at the inlet boundary $\Gamma_{\text{in}}$, which depends on the coordinates $\Gamma_{xyz}$ and the average inlet velocity $v_{\text{in,ave}}$.

The inlet velocity profile that is used ($\boldsymbol{v}_0\left(\Gamma_{xyz}, v_{\text{in,ave}}\right)$) is given differently depending on each numerical example. In the case of considering a fully developed flow condition, the fully developed flow condition from COMSOL Multiphysics® is imposed, which determines the inlet velocity profile by solving for the fluid flow in an extension of the inlet boundary ("inlet channel", with length ten times the inlet edge length in 2D, and length ten times the square root of the inlet area in 3D) while imposing zero tangential velocity ($\boldsymbol{v} - (\boldsymbol{v}\cdot\boldsymbol{n})\boldsymbol{n} = \boldsymbol{0}$) on $\Gamma_{\text{in}}$. The constrained pressure value at the outlet boundary $\Gamma_{\text{out}}$ is given by Eq. (16). The laminar sublayers at the fluid walls are not resolved when wall functions are imposed. Thus, fluid velocity at walls is non zero when a turbulent fluid flow is solved.

The turbulent flow settings for the inlet $\Gamma_{\text{in}}$ are the turbulent intensity $I_T$ and turbulence length scale $L_T$, which are related to the turbulence variables via the following equations (COMSOL 2019):

$$k = \frac{3}{2}\left(|\boldsymbol{v}|I_T\right)^2 \qquad \text{and} \qquad \varepsilon = C_\mu^{3/4}\frac{k^{3/2}}{L_T}, \qquad \text{on } \Gamma_{\text{in}}, \tag{18}$$

when solving for the $k$-$\varepsilon$ model, and

$$k = \frac{3}{2}\left(|\boldsymbol{v}|I_T\right)^2 \qquad \text{and} \qquad \omega = \frac{\sqrt{k}}{\left(\beta_0^*\right)^{1/4}L_T} \qquad \text{on } \Gamma_{\text{in}}, \tag{19}$$

when solving for the $k$-$\omega$ model. The values $I_T = 0.05$ and $L_T = 0.01$ m are prescribed. For the outlet $\Gamma_{\text{out}}$, the boundary conditions for the turbulence quantities are $\boldsymbol{n}\cdot\nabla k = 0$, $\boldsymbol{n}\cdot\nabla\varepsilon = 0$ and $\boldsymbol{n}\cdot\nabla\omega = 0$.

On the walls $\Gamma_w$, the turbulent kinetic energy is subject to a homogeneous Neumann boundary condition $\boldsymbol{n} \cdot \nabla k = 0$ (COMSOL 2019). When solving the $k$-$\varepsilon$ equations, the boundary condition for $\varepsilon$ is given by

$$\varepsilon = \frac{C_\mu^{3/4} k^{3/2}}{\kappa_V \delta_w^+} \qquad \text{on } \Gamma_w. \tag{20}$$

When solving for the $k$-$\omega$ model the boundary condition for $\omega$ at the walls is given by

$$\omega_w = \frac{\rho_f k}{\kappa_V \delta_w^+ \mu} \qquad \text{on } \Gamma_w. \tag{21}$$

### 2.2 Material model

The Brinkman equations (Brinkman 1947) inspire adding friction forces by considering that low permeability regions represent solid domains and high permeability regions represent the domains where the fluid is free to flow. The supplementary forces are added to enforce zero or near-zero velocities in the solid domains in standard fluid flow topology optimization. These forces' magnitude is controlled by the maximum inverse permeability value present in the material model function. The standard topology optimization methods become then quite dependent on the choice of this value, often leading to poorly-performing local minima (Pizzolato 2018). Sometimes, this issue is only solved by an endless and frustrating parameter tuning. Herein, by using the trimming geometry procedure, the effects of adding the material model are low. This is explained by looking into the linear interpolation scheme used in this work, given as

$$\kappa(\alpha) = \kappa_{\max}(1 - \alpha), \tag{22}$$

where $\kappa_{\max}$ is the maximum inverse permeability value. In practice, for the proposed geometry trimming method, it is employed $\kappa_{\max} = 1\ \mathrm{kg/(m^3{\cdot}s)}$, i.e. $\kappa_{\max}$ is not actually used; however, the term is included in Eq. (22) for the comparison against the standard permeability approach analysis carried out in Sect. 5.1. In summary, when $\alpha = 1$, the interpolation scheme leads to $\kappa(\alpha) = 0$, and Eq. (1) becomes the original RANS equations without the interpolation term. In the geometry trimming procedure, the regions where $\alpha = 0$ are trimmed out of the FE analysis domain, creating a CAD geometry that only models the regions where $\alpha = 1$. Therefore, the addition of the interpolation term in the RANS and turbulence equations is not active in the point of view of the fluid flow analysis that is performed in the trimmed geometry. The interpolation scheme is employed only to aid the sensitivity analysis. The same would be valid if the traditional term by Borrvall and Petersson (2003) was used.

This work is the first attempt to carry out turbulent fluid flow topology optimization using binary design variables. The $k$-$\varepsilon$ and $k$-$\omega$ turbulence models are chosen to illustrate that the proposed method might work regardless of the turbulence model. The authors advocate that, when it comes to binary $\{0, 1\}$ topology designs, the choice of the physics modelling is a matter of the application, as there is no interference of material interpolation, as described above. Therefore, the methodology proposed in this work may be directly extended to other fluid flow physics or conditions.

## 3 Topology optimization framework

### 3.1 Optimization problem

In this work, the total fluid energy dissipation (considering the viscous and turbulent effects) is minimized subject to a volume constraint. The total fluid energy dissipation is given by (Borrvall and Petersson 2003; Yoon 2016)

$$\begin{aligned}\Phi(\boldsymbol{u}, \alpha) = &\\ &\int_{\Omega_f} (\mu + \mu_T)(\nabla \boldsymbol{v} + (\nabla \boldsymbol{v})^T) \cdot (\nabla \boldsymbol{v} + (\nabla \boldsymbol{v})^T) d\Omega_f \\ &+ \int_{\Omega_f} \kappa(\alpha) \boldsymbol{v} \cdot \boldsymbol{v} d\Omega_f,\end{aligned} \tag{23}$$

where $\boldsymbol{u}$ is being used to represent the state vector, which includes the velocity ($\boldsymbol{v}$), pressure ($p$) and turbulence variables ($k$ and $\varepsilon$, or $k$ and $\omega$, depending on the turbulence model).

The topology optimization formulation can then be expressed as

$$\begin{aligned}&\underset{\alpha}{\text{Minimize}}\ \Phi(\boldsymbol{u}(\alpha), \alpha) \\ &\text{Subject to } V_\alpha \leqslant \overline{V} \\ &\qquad\qquad \alpha. \in \{0, 1\}\end{aligned} \tag{24}$$

where $\boldsymbol{u}(\alpha)$ is the state vector computed for a given design variable distribution $\alpha$, $V_\alpha = \int_\Omega \alpha \mathrm{d}\Omega$ is the fluid volume computed for a given design variable distribution $\alpha$, $\overline{V} = f \int_\Omega \mathrm{d}\Omega$ is the constrained fluid volume, and $f$ is the maximum allowed fluid volume fraction.

### 3.2 Sensitivity analysis

The TOBS method is a gradient-based algorithm, meaning that the derivatives (sensitivities) of the objective function and constraints are required. A general way of computing the sensitivity of the objective function $\Phi$ is via the adjoint method (Haftka and Gürdal 1992). The adjoint equation is then expressed as

$$\left(\frac{\partial \mathbf{R}}{\partial \boldsymbol{u}}\right)^T \lambda = -\left(\frac{\partial \Phi}{\partial \boldsymbol{u}}\right)^T, \tag{25}$$

where $\lambda$ is the adjoint variable, $\Phi$ is the objective function and $\boldsymbol{R}$ is the residual (given from the weak formulation of the fluid flow problem). Therefore, the sensitivity $\frac{\mathrm{d}\Phi}{\mathrm{d}\alpha}$ can be computed as

$$\frac{\mathrm{d}\Phi}{\mathrm{d}\alpha} = \frac{\partial \Phi}{\partial \alpha} + \lambda^T \frac{\partial \mathbf{R}}{\partial \alpha}. \tag{26}$$

The sensitivity of the volume constraint depends on $V_\alpha$. The discrete form of $V_\alpha = \int_\Omega \alpha \mathrm{d}\Omega$ is given as

$$V_\alpha = \sum_{j=1}^{N_d} \alpha_j V_j, \tag{27}$$

where $V_j$ is the volume of the element $j$, $\alpha_j$ is the value of the design variable in the element $j$, and $N_d$ is the total number of elements. Then, the sensitivity of this term is given in the discrete form as:

$$\frac{\mathrm{d}V_\alpha}{\mathrm{d}\alpha_j} = V_j. \tag{28}$$

### 3.3 TOBS method

The TOBS (Topology Optimization of Binary Structures) method is based on sequential approximations to integer linear optimization subproblems and on their solutions. By representing the design variable ($\alpha$) in its discrete form ($\boldsymbol{\alpha}$), and by considering a Taylor's series expansion and truncating its first term (linear part), the objective function and volume constraint can be expressed as follows, for the optimization iteration $n$:

$$\begin{aligned} \Phi(\boldsymbol{\alpha}) &\approx \Phi(\boldsymbol{\alpha}^n) + \frac{\mathrm{d}\Phi(\boldsymbol{\alpha}^n)}{\mathrm{d}\boldsymbol{\alpha}} \cdot \Delta\boldsymbol{\alpha}^n + O(\left|\left|\Delta\boldsymbol{\alpha}^n\right|\right|_2^2), \\ V_\alpha(\boldsymbol{\alpha}) &\approx V_\alpha(\boldsymbol{\alpha}^n) + \frac{\mathrm{d}V_\alpha(\boldsymbol{\alpha}^n)}{\mathrm{d}\boldsymbol{\alpha}} \cdot \Delta\boldsymbol{\alpha}^n + O(\left|\left|\Delta\boldsymbol{\alpha}^n\right|\right|_2^2), \end{aligned} \tag{29}$$

where the truncation error is given as $O(\left|\left|\Delta\boldsymbol{\alpha}^n\right|\right|_2^2)$, and $\Delta\boldsymbol{\alpha}^n$ is the vector that represents the changes in the design variable. The changes in the design variable should be restricted in order to keep the design variable with integer (i.e., binary) values. For example, by considering an element that contains a fluid material ($\alpha_j = 1$), the changes in the design variable can be restricted as $\Delta\alpha_j \in \{-1, 0\}$, meaning that this element may either turn into a solid material ($\alpha_j = 0$) or keep its value ($\alpha_j = 1$) in the optimization iteration. The same procedure is analogous for an element that contains a solid material ($\alpha_j = 0$). The bound constraints for $\Delta\alpha_j$ can then be expressed as,

$$\begin{cases} 0 \leqslant \Delta\alpha_j^n \leqslant 1 & \text{if } \alpha_j^n = 0, \\ -1 \leqslant \Delta\alpha_j^n \leqslant 0 & \text{if } \alpha_j^n = 1, \end{cases} \tag{30}$$

or, in a unified form,

$$\Delta\alpha_j^n \in \{-\alpha_j^n, 1 - \alpha_j^n\}, \tag{31}$$

where $\Delta\alpha_j^n \in \{-1, 0, 1\}$. In order to maintain the linear approximation from Eq. (29) valid, the truncation error $O(\left|\left|\Delta\boldsymbol{\alpha}^n\right|\right|_2^2)$ should be sufficiently small. The value of the truncation error is controlled by including an additional constraint to the optimization subproblem, which restricts the number of "flips" of $\boldsymbol{\alpha}^n$ from 1 to 0 and vice-versa. The truncation error constraint can be expressed as

$$\left|\left|\Delta\boldsymbol{\alpha}^n\right|\right|_1 \leqslant \beta N_d. \tag{32}$$

In topology optimization, the truncation error constraint given by Eq. (32) means that the number of elements that may turn from fluid to solid and vice-versa is restrained to a fraction ($\beta$) of the total number of elements ($N_d$). By using small values of the fraction $\beta$, the number of flips is ensured to be kept low at each iteration $n$, meaning that the truncation error is also kept small.

By considering the sequential linear approximations from Eq. (29), the integer variable constraint from Eq. (31), and the truncation error constraint from Eq. (32), the approximate integer linear subproblem is given as

$$\begin{aligned} &\underset{\Delta\boldsymbol{\alpha}^k}{\text{Minimize}} \ \frac{\mathrm{d}\Phi(\boldsymbol{\alpha}^n)}{\mathrm{d}\boldsymbol{\alpha}} \cdot \Delta\boldsymbol{\alpha}^n, \\ &\text{Subject to} \ \frac{\mathrm{d}V_\alpha(\boldsymbol{\alpha}^n)}{\mathrm{d}\boldsymbol{\alpha}} \cdot \Delta\boldsymbol{\alpha}^n \leqslant \overline{V} - V_\alpha\left(\boldsymbol{\alpha}^n\right) := \Delta V_\alpha^k, \\ &\qquad \left|\left|\Delta\boldsymbol{\alpha}^n\right|\right|_1 \leqslant \beta N_d, \\ &\qquad \Delta\alpha_j^n \in \{-\alpha_j^n, 1 - \alpha_j^n\}, \ j \in [1, N_d]. \end{aligned} \tag{33}$$

Eq. (33) shows the sequential optimization subproblems in the standard TOBS formulation, where the truncation error constraint (Eq. (32)) restrains the topology from undergoing great changes. However, when the constraint is bounded with $\Delta V_\alpha^n = \overline{V} - V_\alpha\left(\boldsymbol{\alpha}^n\right)$, the constraint may possibly become infeasible in the current optimization iteration $n$. This undesirable effect may be avoided by modifying the bound of the constraint ($\Delta V_\alpha^n$) such that the optimization subproblems yield feasible solutions. This approach also helps in generating feasible subproblems when the initial guess of the design variable is distant from feasibility – for instance, when the initial guess consists of a "fully-fluid" design domain whilst having a small allowed fluid volume fraction ($f$). Therefore, the constraint bounds are modified by considering

$$\Delta V_{\alpha}^{n} = \begin{cases} -\epsilon V_{\alpha}\left(\boldsymbol{\alpha}^{n}\right) & : \overline{V} < (1-\epsilon)V_{\alpha}\left(\boldsymbol{\alpha}^{n}\right), \\ \overline{V} - V_{\alpha}\left(\boldsymbol{\alpha}^{n}\right) & : \overline{V} \in [(1-\epsilon)V_{\alpha}\left(\boldsymbol{\alpha}^{n}\right), (1+\epsilon)V_{\alpha}\left(\boldsymbol{\alpha}^{n}\right)], \\ \epsilon V_{\alpha}\left(\boldsymbol{\alpha}^{n}\right) & : \overline{V} > (1+\epsilon)V_{\alpha}\left(\boldsymbol{\alpha}^{n}\right), \end{cases} \tag{34}$$

where $\epsilon$ is the relaxation parameter corresponding to the constraint given by $V_{\alpha}$. Although the TOBS formulation is being described for a single constraint, more constraints can be considered (Picelli et al. 2020b; Sivapuram et al. 2018), and any other differentiable function can be used as a constraint (Picelli et al. 2020b; Sivapuram et al. 2018).

The integer optimization subproblems generated by using sequential linearizations (Eq. (33)) can be solved through Integer Linear Programming (ILP). An ILP problem is essentially the same as a Linear Programming (LP) problem, but imposing additional constraints to ensure that the design variables can only achieve integer values. Therefore, ILP-based solutions become suboptimal with respect to the LP-based solutions. Nevertheless, since fluid topology optimization aims to achieve a binary ($\{0, 1\}$) solution, the use of integer programming should be naturally understandable. In this work, the ILP problem is solved by using the branch-and-bound algorithm from the CPLEX® optimization library, which is developed by IBM®. The branch-and-bound method consists of an algorithm based on a tree data structure, in which the ILP problem is first solved without any integer constraints (by using a linear optimization technique such as the Simplex method); then, branches of LPs are created with additional inequality constraints being imposed on the design variables in order for the solution to be yielded as integer (Land and Doig 1960; Vanderbei 2014). Sivapuram and Picelli (2020) present a study that indicated that the computational time required by the ILP solver and by the FEA increases, linearly and exponentially with the mesh size, respectively, for the traditional fixed grid approach; hence, the bottleneck of the optimization is still the FEA.

## 4 Numerical implementation

### 4.1 Details of FEA software setup

The RANS equations (Eqs. (1) and (2)) including the $k$-$\epsilon$ (Eqs. (4) and (5)) and $k$-$\omega$ (Eqs. (12) and (13)) turbulence models with wall functions are solved via the commercial FEA software COMSOL Multiphysics®. For convection-dominated transport problems, the FEA may lead to numerical instabilities, namely, oscillations in the solution. In order to prevent this phenomenon, the Streamline and Crosswind Diffusion stabilizations are applied.

The interpolation function from Eq. (22) is employed via COMSOL's Topology Optimization module. The penalization terms related to $\kappa(\alpha)$ are implemented as body forces on the fluid flow domain for the RANS and turbulence equations.

### 4.2 The TOBS-GT method

The proposed methodology is based on the decoupling of the optimization grid and the FEA mesh. The process is illustrated in Fig. 3. The fluid flow and sensitivity analyses are carried out using COMSOL Multiphysics®. First, a CAD model is created with the analysis domain. The geometry is then freely meshed by using the option `physics controlled` in COMSOL Multiphysics®. The option takes into account some built-in physics requirements when meshing. This choice can be of some benefit when dealing with complex fluid flow, which is a problem that requires certain levels of mesh refinement at the walls, or even different types of elements for the boundary layers. The forward and adjoint problems are solved, computing velocities, pressures and sensitivities. These three entities are computed using nodal variables at the finite element software. The sensitivities are obtained via automatic differentiation. After that, optimization grid is created and the sensitivities are interpolated at the TOBS-GT optimization points. The finite element shape functions can be used to interpolate the sensitivities at such points. Standard spatial filtering (Picelli et al. 2020b) is applied at the sensitivities defined at the optimization (structured) grid. The ILP solver is then used to find a new set of binary design variable values. The new topology is then used at the next iteration. Besides the analysis domain, the contours of the holes defined by the binary variables are first identified and stored in points coordinates, creating a staircase contour. Then, the contour coordinates are filtered to create a smooth representation. In 2D, the smoothing is carried out by using the Savitzky–Golay filter (Savitzky and Golay 1964), and in 3D, by the Shrink Wrap tool from ANSYS. The smooth contours are saved (as `.dxf` for 2D and `.stl` for 3D problems) and provided to the FEA package. A new CAD model can be created by trimming out the holes from the analysis domain. This is carried in the geometry building section from COMSOL Multiphysics® with the command `difference`. In this way, the modeled solid regions, usually modeled with the inverse permeability term in traditional methods, are not considered in the simulation. This procedure eliminates the influence of the maximum inverse permeability value. Another benefit of decoupling the optimization variables and the FEA is that the optimization grid can be relatively coarse and still produce crisp topologies with smooth walls while the FEA mesh can be also maintained in a certain size with a relatively low computational cost. The authors advocate that the TOBS-GT should be a general idea. Other new or standard tools can be incorporated in the methodology according to convenience, e.g., in the FEA solution, the type of sensitivity

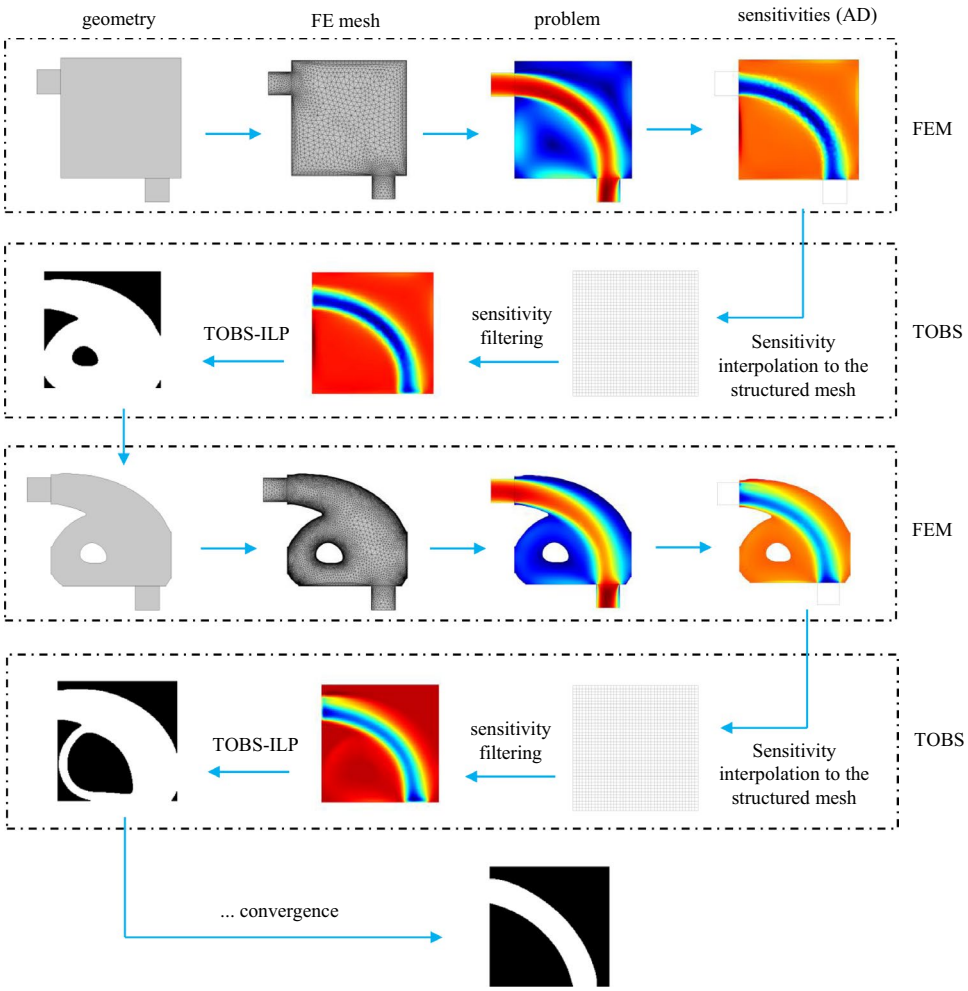


**Fig. 3** Illustration of the TOBS with geometry trimming procedure (TOBS-GT) applied to fluid flow design. The illustration shows a few of the intermediate optimization steps until the convergence

analysis, different physics applications or techniques for wall smoothing.

### 4.3 Sensitivity computation

The forward problem is computed with a stationary study solver added by the sensitivity module in COMSOL Multiphysics® for computing the sensitivities from automatic differentiation.

The fluid energy dissipation function can be written directly in the software and coupled to an integration operator defined over the analysis domain. The sensitivities concerning the material model can be extracted via `fsens(dtopo1.theta_c)/dvol`. In COMSOL Multiphysics®, the variable `theta_c` is used to represent the vector of design variables ("$\boldsymbol{\alpha}$"). The sensitivities computation is done considering the averaging of the element volumes for mesh independence purposes. A set of grid points coincident with the optimization grid can be created to extract the sensitivities at those points and then carry out the communication between the FEA and the optimization, as illustrated in Fig. 3. Sensitivities for points in the (trimmed out) solid regions are zero as no physical analysis is carried out for those regions. Regardless, in this flow channel problem, they should also be zero for the standard inverse permeability approach as the fluid velocities should tend to zero in those regions. Herein, the sensitivities in the FEA software are output as `NaN` and substituted by zero before passing them to the optimizer. Back to the optimization module, the spatial filtering is used in the sensitivity field, populating the solid regions outside the FEA domain with sensitivities.

### 4.4 Algorithm

In summary, the algorithm of the proposed TOBS-GT method is the following:

1. Define the optimization parameters.
2. Create the optimization grid and assign an initial $\{0, 1\}$ topology.

3. Extract and smooth the topology contours and save holes' contour information (if any) as `.dxf` (for 2D) or `.stl` (for 3D).
4. Define the fluid flow problem in CAD and create initial geometry.
5. Trim the CAD geometry with holes contours information (if any) and create the fluid flow analysis domain.
6. Mesh the trimmed geometry.
7. Solve the RANS equations (including turbulence wall functions).
8. Extract sensitivities in a grid coincident with the optimization grid.
9. Apply spatial filtering on the sensitivity field considering the optimization grid position.
10. Solve the linearized optimization subproblem from Eq. (24) with the branch-and-bound algorithm.
11. Update design variables to build a new $\{0, 1\}$ topology.
12. If converged, stop. If not, iterate from step 3.

In this work, the steps from 4 to 8 are carried out in COMSOL Multiphysics®, while the others are done in MATLAB® using the TOBS implementation available at www.github.com/renatopicelli/tobs.

## 5 Numerical results

This section presents numerical results and discussions on the application of the proposed TOBS-GT method. First, a comparison against the standard fluid flow optimization with inverse permeability is carried out for low Reynolds regime, as it does not require wall functions. Then, 2D and 3D turbulence examples with geometry trimming are explored.

### 5.1 Investigation of the geometry trimming approach

The U-bend design problem illustrated in Fig. 4 is chosen for optimization. A similar example was investigated by Dilgen et al. (2018a). Herein, the U-bend is first used to verify the proposed geometry trimming approach against the standard inverse permeability methodology for low Reynolds flow regime. The fluid enters the inlet boundary $\Gamma_{\text{in}}$ with a fully developed flow condition and average velocity computed as function of the Reynolds number Re as

$$v_{\text{in,ave}} = \frac{\text{Re} \cdot \mu}{\rho_{\text{f}} \cdot \text{H}}, \tag{35}$$

where H is the characteristic length of the flow. The fluid should make a U-turn around the "always solid" stem in the center and exit through the outlet $\Gamma_{\text{out}}$, which is set for $p_{\text{out}} = 0$. The fluid is considered to have dynamic viscosity $\mu = 5 \cdot 10^{-5}$ Pa s and density $\rho_{\text{f}} = 1\,\text{kg/m}^3$. In the standard

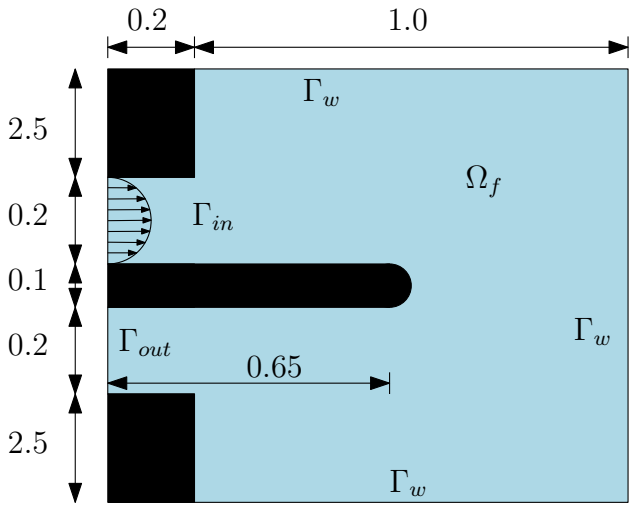


**Fig. 4** U-bend example. Regions in black color are modeled with the inverse permeability term and fixed as solid material. Dimensions in m

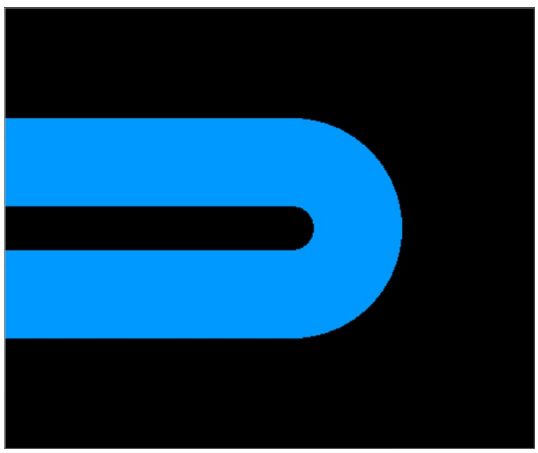

**Fig. 5** Baseline solution for the U-bend example used as initial guess design

fluid flow topology optimization (Borrvall and Petersson 2003), the solid regions are modeled with the inverse permeability term introduced in Eq. (22). In the present TOBS-GT method, these regions are trimmed out and only the analysis domain has the inverse permeability for sensitivity calculation purposes.

To understand the effect of trimming the solid regions out of the analysis, the U-bend is optimized with the standard TOBS approach with inverse permeability and initial guess from Fig. 5 for different values of $\kappa_{\text{max}}$. For better comparison, the Reynolds number used is 300, i.e., the fluid flow is assumed to be in the low Reynolds regime ($\mu_T = 0$). The characteristic length used is H = 0.2 m, the same size as the inlet. The TOBS parameters are $\epsilon = 0.01$

and $\beta = 0.05$ and the maximum allowed fluid volume fraction is set as $f = 0.30$. The optimized topologies obtained by using the inverse permeability approach are presented in Figs. 6a–c for different values of $\kappa_{\max}$. For the case with trimmed geometry, given in Fig. 6d, $\kappa_{\max} = 1$ kg/(m$^3$·s). By comparing the inverse permeability results with the trimmed geometry solution, it is possible to observe that the geometry trimming solution tends to be equivalent to running the optimization with a high inverse permeability. Hence, the advantage of the TOBS-GT method is that the topology optimization analysis does not require selecting and testing for various $\kappa_{\max}$ values. Besides, a large area of solid region is not unnecessarily solved in the FEA. Figure 7 presents the CAD geometry and the velocity and pressure fields for the solution obtained with the geometry trimming procedure.

The solutions for the U-bend topology optimization from both the standard TOBS with inverse permeability and the TOBS-GT method are asymmetric according to Fig. 6. The topologies present an asymmetry about the horizontal axis cutting the pipe halfway. To verify that this asymmetry is indeed optimal, the optimization is also run by enforcing symmetry and the result is presented in Fig. 8b. By checking the objective function values for the asymmetric ($\Phi = 3.88 \cdot 10^{-5}$ W/m) and the symmetric solution ($\Phi = 4.44 \cdot 10^{-5}$ W/m), it is possible to see that the asymmetric solution presents less energy dissipation and the asymmetry is not induced by the optimization algorithm.

## 5.2 Two-dimensional turbulence problems

The previous example explored the fluid flow optimization in the low Reynolds regime as the standard inverse permeability approach only emulates the fluid boundaries and it is currently unable to include wall functions. In this subsection, topology optimization is carried out for turbulent fluid flow using the proposed TOBS-GT method, which is suitable for the inclusion of turbulence wall functions.

### 5.2.1 Pipe-bend

The pipe-bend example illustrated in Fig. 9 is chosen as a benchmark for the geometry trimming procedure. The fluid $\Omega_f$ flows through the inlet $\Gamma_{in}$ with a fully developed flow condition and exits via the outlet $\Gamma_{out}$ with $p_{out} = 0$. The fluid is considered to have dynamic viscosity $\mu = 4 \cdot 10^{-5}$ Pa s and density $\rho_f = 1$ kg/m$^3$. The $k$–$\epsilon$ turbulence model is employed. The design domain is considered to be the 1 m × 1 m domain.

The TOBS-GT method is applied with optimization parameters $\epsilon = 0.01$ and $\beta = 0.02$ and maximum allowed fluid volume fraction is set as $f = 0.2513$, the same area of a quarter torus of inner radius 0.7 m and outer radius 0.9 m that fits to the inlet and outlet of the pipe-bend. The TOBS-GT optimization grid is chosen to be 200×200. For Re = 5000 and characteristic length H = 0.2 m, Fig. 10 presents the snapshots of the pipe-bend optimization, including the velocity field plots. The proposed TOBS-GT method decouples the optimization grid from the finite element mesh. Figure 11a presents the zoomed details of the optimization grid.

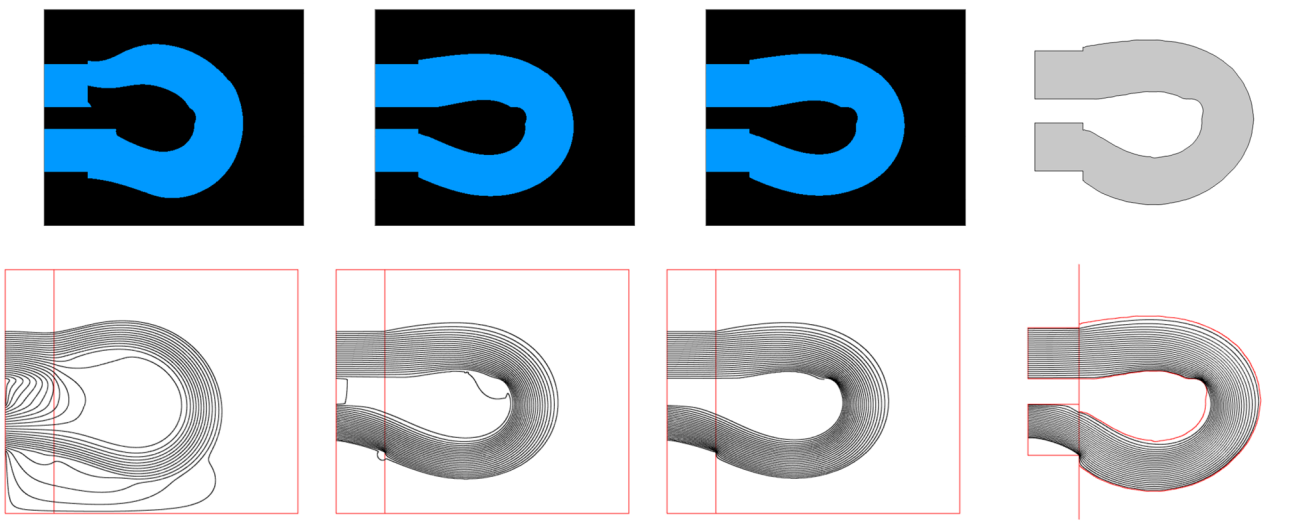

(a) $\kappa_{max} = 1$ kg/(m$^3$·s). (b) $\kappa_{max} = 10^2$ kg/(m$^3$·s). (c) $\kappa_{max} = 10^4$ kg/(m$^3$·s). (d) Geometry trimming, $\kappa_{max} = 1$ kg/(m$^3$·s).

**Fig. 6** Effect of $\kappa_{\max}$ on the U-bend optimization problem: **a**–**c** using the standard TOBS with inverse permeability and **d** using the proposed TOBS-GT method for Re = 300, showing topology solutions and velocity field streamlines

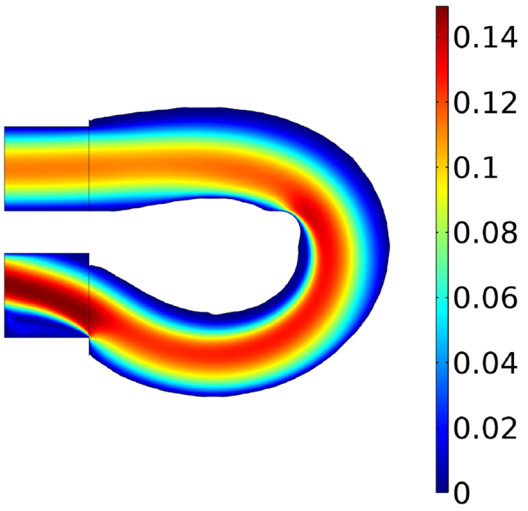


(a) Fluid velocity field (in m/s).

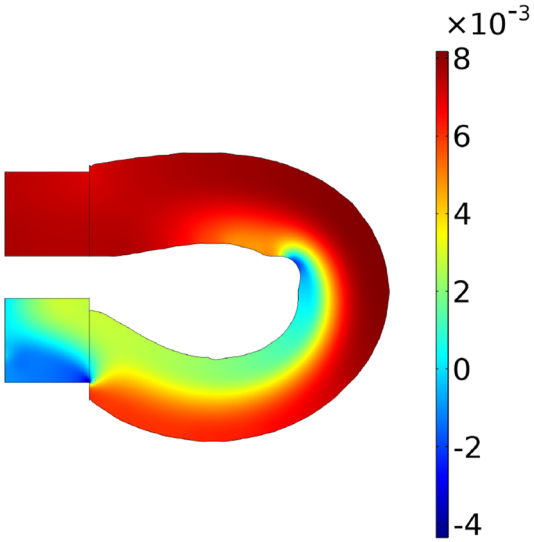


(b) Fluid pressure field (in Pa).

**Fig. 7** U-bend topology optimization obtained by the TOBS-GT method for Re = 300

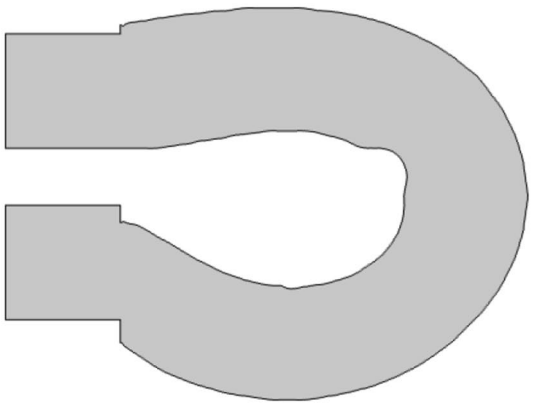

(a) $\Phi = 3.88 \cdot 10^{-5}$ W/m.

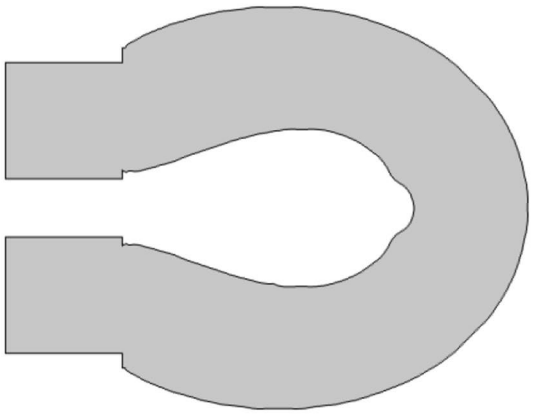

(b) $\Phi = 4.44 \cdot 10^{-5}$ W/m.

**Fig. 8** U-bend topology optimization obtained by the TOBS-GT method for Re = 300: **a** regular solution and **b** solution obtained when enforcing symmetry

A CAD model (shown in Fig. 11b) is created after extracting the smoothed contours of the $\{0, 1\}$ design defined in the optimization grid. Finally, a convenient finite element mesh is generated for the fluid dynamics calculations. This represents a new surface-capturing method for topology optimization. Although some of its features are similar to body-fitted level set methods, the TOBS-GT is still in the digital $\{0, 1\}$ optimization framework.

The pipe-bend example from Fig. 10 was optimized via the TOBS-GT method in a total time of 3.33 hours using an Intel Xeon Silver 4114 - 2x CPU 2.20 GHz - 128 GB RAM. Figure 12a shows the breakdown times for all steps in the TOBS-GT method. It can be seen that the FEA solver (forward and adjoint problems) requires the largest computation time, similarly as for other standard methods. The times required by the FEA solver varies along the iterations, which might be explained by looking at the fluid walls and flow complexities. As seen in Fig. 10a–d, the intermediate topologies present more holes due to fluid flow recirculation zones, behaviour that goes until around iteration 70 in the optimization, point where the FEA solver started to require less computational time. The same is observed for the generated finite element mesh, as it can be seen in Fig. 12b. Until iteration 60, the times for the finite element mesh generation were in average about 3 seconds due to the complexity of the CAD model. Another novel and important point of the present method is the use of an ILP solver. This step required

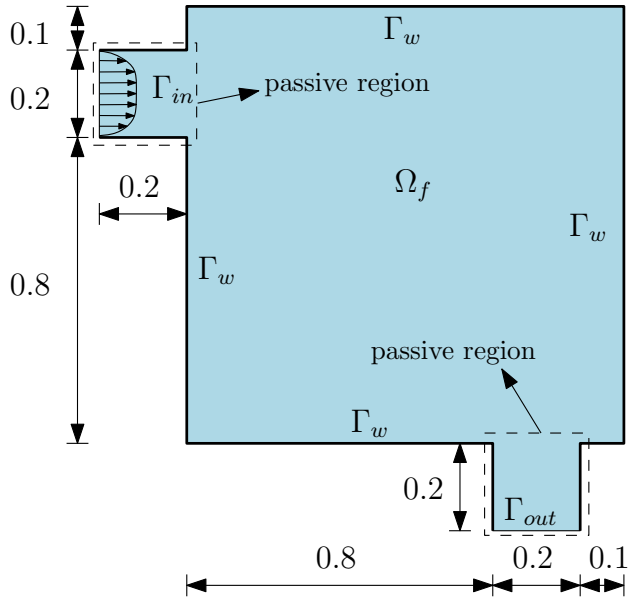


**Fig. 9** Pipe bend example. Dimensions in m

less than a second per iteration to solve for 40,000 binary variables. Therefore, ILP is feasible for topology optimization in the present TOBS-GT method.

In our numerical experience, the TOBS-GT method shows the tendency of reaching similar minima. To illustrate that, Fig. 13 presents the optimization of the pipe-bend example starting with an initial guess design of a fluid flow around a square solid. It can be seen that the optimizer starts with the removal of the bottom left passage, while later on it shapes the flow path and converges to the same solution as in Fig. 10, but with 90 iterations. Figure 14 presents the convergence history of both pipe-bend optimizations. Larger variations can be observed in the case starting with the initial full fluid, possibly explained by the changes in the smooth boundaries locations. For the case with an initiall guess design, the convergence was relatively smooth.

Although the pipe-bend is a simple benchmark example, only Yoon (2016) previously presented solutions for this problem, surprisingly. In general, it seems that the designs in Yoon (2016) tend to connect the inlet and outlet in a straight pipe but with some curved shapes. Fairly, when an outlet tube is used, a curved pipe design is obtained, more similarly to these present solutions.

### 5.2.2 U-bend

The U-bend design problem from Sec. 5.1 is explored here, however now solely with the geometry trimming procedure and turbulence models. Three different types of inlet/outlet configurations are explored for the U-bend example, namely, a case with a smaller outlet tube, a case with neither inlet nor outlet tubes and a case with a larger outlet tube. These cases are illustrated in Fig. 15. In all U-bend's, the fluid $\Omega_f$ flows through the inlet $\Gamma_{in}$ with a fully developed flow

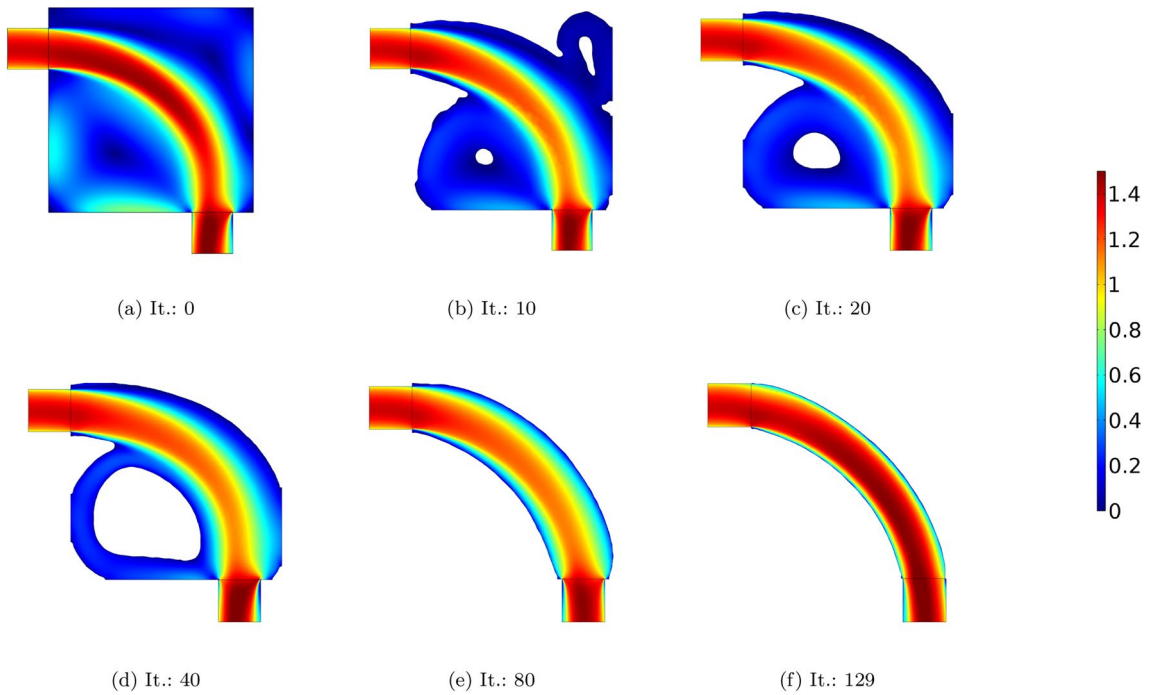


**Fig. 10** Pipe-bend example optimized with the TOBS-GT method for minimum fluid energy dissipation. Velocity field in m/s

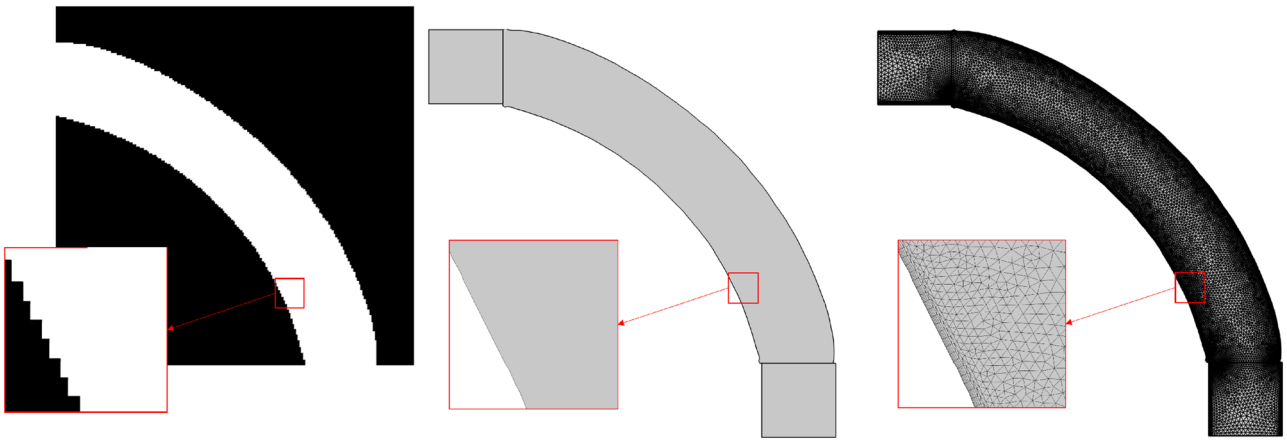

(a) $\{0, 1\}$ design in the optimization grid (b) CAD model. (c) Finite element mesh.

**Fig. 11** Zoomed details of the **a** $\{0, 1\}$ design optimized in a $200 \times 200$ fixed grid, **b** CAD model created via the smoothed topology contours and (c) freely generated finite element mesh (26257 triangular, 4111 quadrilateral, 992 edge and 646 vertex elements)

condition and exits via the outlet $\Gamma_{\text{out}}$ with $p_{\text{out}} = 0$. The fluid is considered to have dynamic viscosity $\mu = 4 \cdot 10^{-5}$ Pa s and density $\rho_{\text{f}} = 1\,\text{kg/m}^3$. The TOBS-GT method is applied with optimization parameters $\epsilon = 0.01$ and $\beta = 0.05$ and maximum allowed fluid volume fraction $f = 0.27$, the same area of the baseline design showed in Fig. 5. The optimization grid is chosen to be $200 \times 200$. The problem is solved with both turbulence models $k$-$\varepsilon$ and $k$-$\omega$. The Reynolds number is first set to Re = 5000, when computing it with characteristic length H = 0.2 m. Fig. 16 presents the velocity (in m/s) and pressure (in Pa) fields for the optimized U-bend optimized topologies using the case with smaller outlet tube and for both $k$-$\varepsilon$ and $k$-$\omega$ turbulence models. This is similar to the case investigated by Dilgen et al. (2018a).

Although the topology solutions presented in Fig. 16a and b are somehow similar between each other, noticeable differences appear in the fluid wall locations and the fluid flow responses due to the chosen governing equations. In contrast to $k$-$\varepsilon$, the solution obtained using the $k$-$\omega$ turbulence model shows the tendency of disconnecting the flow from the upper side of the stem wall, obtaining a wider turn around the stem. This also observed for the other solutions obtained in this work using $k$-$\omega$. It can be pointed out that, in this example, a small layer of optimization pixels were kept fixed in the connection zone between the inlet/outlet tubes and the design domain. This, in combination with the smoothing wall filter, ensured a smooth connection between those regions, differently from the design showed in 8. The solutions in Fig. 16 were obtained defining and computing the objective function only within the 1×1 m design domain. Figure 17a presents the topology obtained when including the inlet and outlet tubes in the objective function evaluation. Both solutions are basically similar, with almost unnoticeable differences in the bottom shapes of the U-bend that cause less recirculation in the outlet when including that region in the objective function computation. Figure 17b and c present the U-bend designs using the $k$-$\varepsilon$ turbulence model for the cases with no tubes and the larger outlet tube, respectively. In the design without inlet/outlet tubes, the flow exits the domain with some inclination. The U-bend solution for the case with the larger outlet tube is more similar to the one with the smaller tube, however, presenting even less recirculation in the beginning of the outlet region, exiting the domain with a fully developed flow profile.

The geometry trimming procedure favors the selection of different fluid flow physics and the combination of the optimization with off-the-shelf finite element packages. This procedure can be particularly advantageous for turbulence problems, as it provides explicitly defined fluid walls and turbulence wall functions can be directly employed. Figure 18 shows the U-bend optimized designs for Re = 5000, Re = 10,000 and 20,000, when using the $k$-$\omega$ turbulence model. As optimization and analysis are decoupled in the TOBS-GT method, increasing the flow velocities do not imply in further challenges for the optimization method itself, but to the convergence of the analysis. In this case, the technical challenges are related only to the CFD side of the problem.

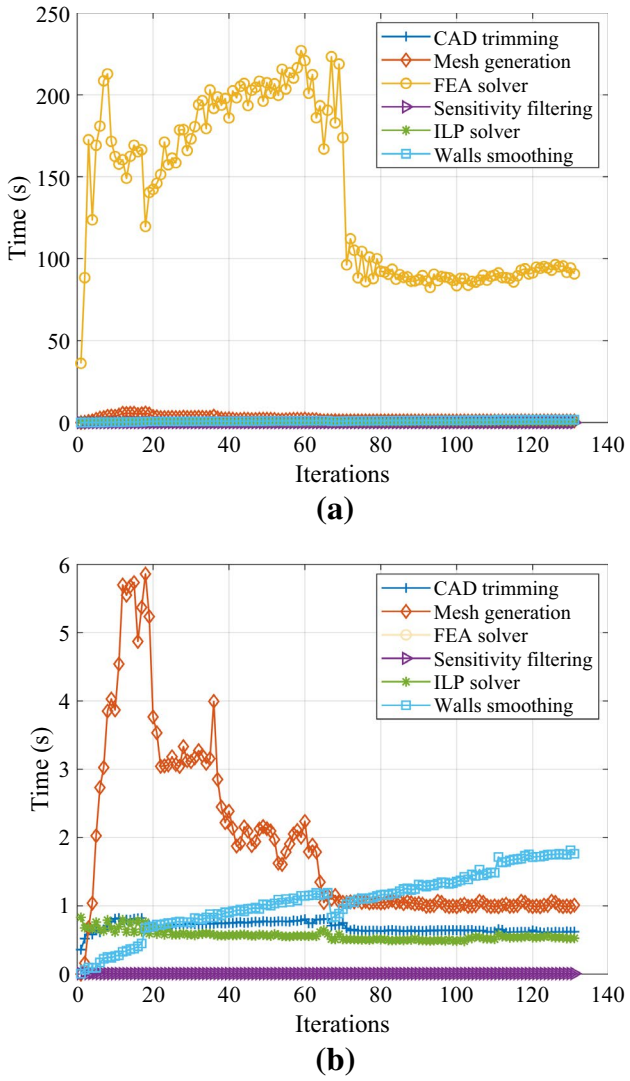


**Fig. 12** Breakdown computation times for the pipe-bend example optimized with the TOBS-GT method: **a** for all steps and **b** omitting the FEA solver times

In order to further check the designs, a cross-check analysis is carried out comparing the U-bend obtained by the TOBS-GT method against the solution with enforced symmetry and the baseline solution for the case with neither inlet/outlet tubes. This symmetric design tends to look more similar to the U-bend designs obtained by Dilgen et al. (2018a) and the baseline solution is chosen as a simpler design connecting the inlet and outlet. The $k$-$\omega$ turbulent flow is used and the Reynolds number is set to be Re = 5000. Fig. 19 presents the described cross-check analysis, including the velocity fields, in m/s, and the local energy dissipation $(\mu + \mu_T)(\nabla \boldsymbol{v} + (\nabla \boldsymbol{v})^T) \cdot (\nabla \boldsymbol{v} + (\nabla \boldsymbol{v})^T)$, in W/m. It is possible to observe that the solution obtained by the TOBS-GT method presents lower energy dissipation. This might be explained by the presence of smaller regions of flow recirculation in the obtained solution and larger regions of local energy dissipation in the symmetric and baseline solutions.

### 5.3 Three-dimensional turbulence problem

The 3D pipe-junction example presented in Fig. 20 is considered for optimization. The example considers two inlets and one outlet with different cross sections as depicted in Fig. 20a. The pipe-junction should be designed inside a cubic domain of 1 m × 1 m × 1 m. The positions of the centroids of the inlet 1, the inlet 2 and the outlet faces touching the cubic design domain are, respectively, (0.35, 0.35, 0.00), (0.25, 1.00, 0.25) and (1.00, 0.50, 0.50), with units in m. The lengths of both inlets and the outlet are 0.2 m. An initial guess design full of fluid as indicated in Fig. 20c is chosen to start the optimization. To produce this initial guess design, the regions that satisfy the following conditions should be trimmed out of the full design domain: ($z > 0.70$), ($x > 0.50$ and $z < 0.30$), ($x > 0.50$ and $y < 0.30$), ($x > 0.50$ and $y > 0.70$), ($x > 0.50$ and $y > 0.70$) and ($y > 0.70$ and $z > 0.50$), in a Cartesian plane $(x, y, z)$ with units in m.

The TOBS-GT method is applied with optimization parameters $\epsilon = 0.05$ and $\beta = 0.10$ and maximum allowed fluid volume fraction $f = 0.20$. A grid of $100 \times 100 \times 100$ optimization points is considered. The fluid is considered to have dynamic viscosity $\mu = 5 \cdot 10^{-5}$ Pa s and density $\rho_f = 1$ kg/m$^3$. The fluid enters the two inlets with constant velocity profile. First, the fluid flow is optimized in the laminar regime with Re = 0,001, when using the characteristic length of H = 0.2 m, and this solution is shown in Fig. 21a. The 3D pipe-junction obtained for the laminar flow is used as initial guess design for the optimization with turbulent flow and Re = 5,000. The $k$-$\epsilon$ turbulence model is employed considering its respective wall function. The final pipe-junction optimized using the turbulent flow is shown in Fig. 21d. It can be seen in Fig. 21 that the optimizer reduces the dimensions of the cross sections connecting the inlets and slightly altered their inclination. This is done to remove the recirculation zones present in the initial guess design when the turbulent

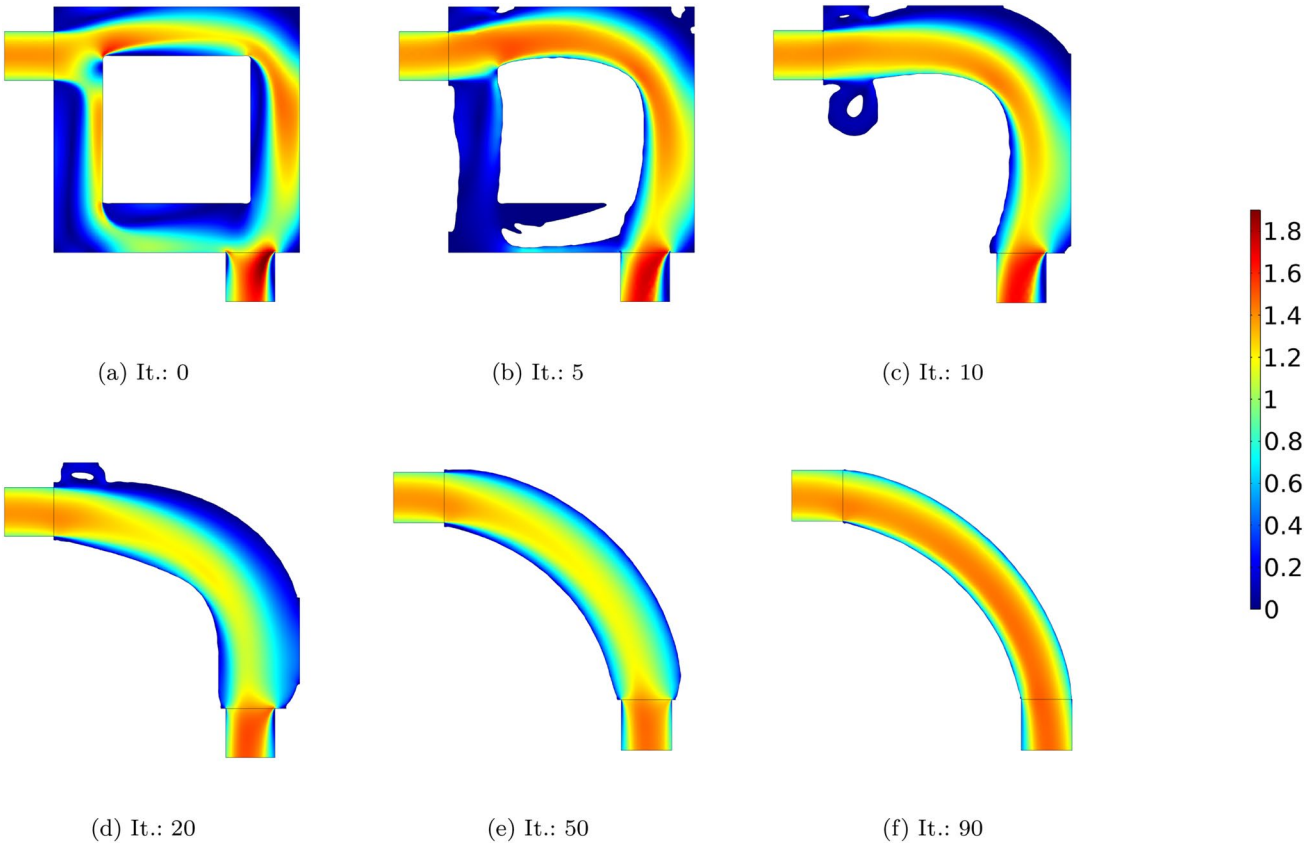


**Fig. 13** Pipe-bend example optimized with the TOBS-GT method for minimum fluid energy dissipation starting with an initial guess design. Velocity field in m/s

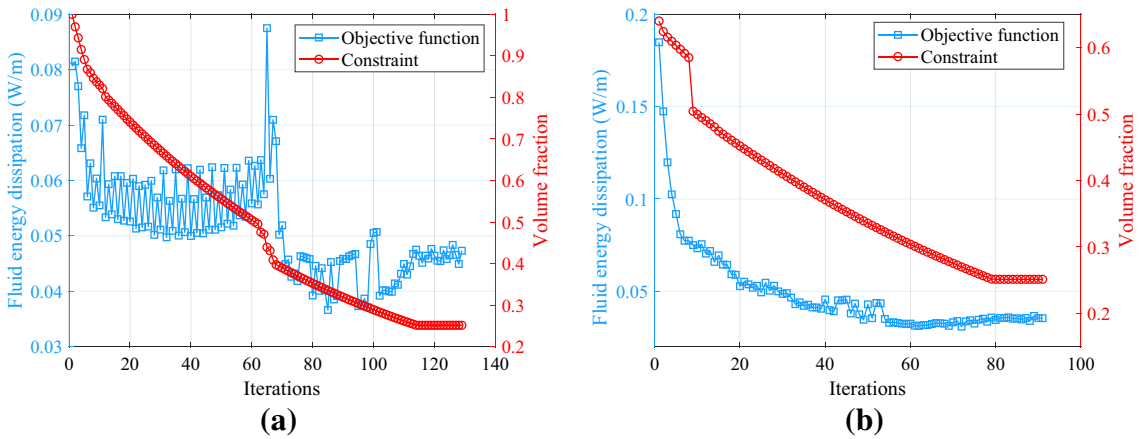


**Fig. 14** Convergence history of the pipe-bend design by the TOBS-GT starting from the **a** full fluid design and **b** initial guess design

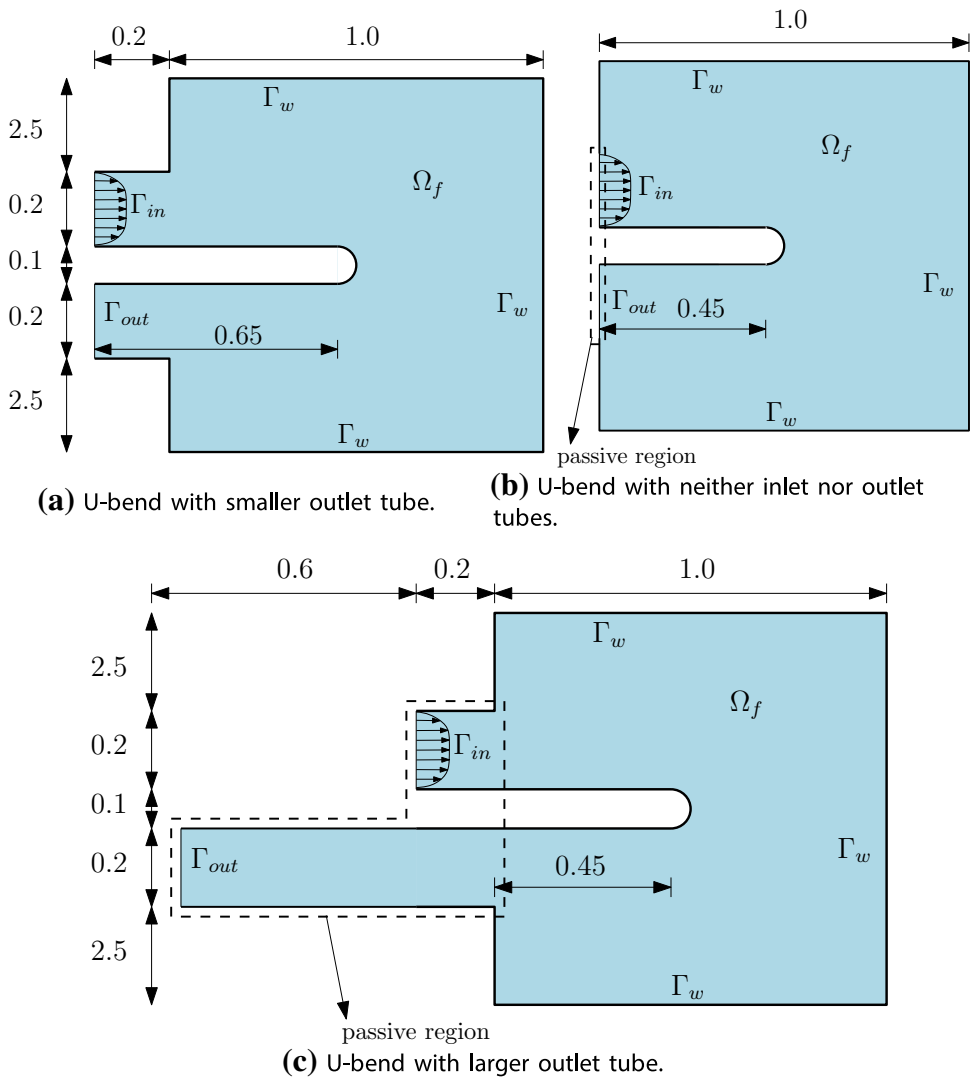


**(a)** U-bend with smaller outlet tube.

**(b)** U-bend with neither inlet nor outlet tubes.

**(c)** U-bend with larger outlet tube.

**Fig. 15** Investigated U-bend configurations. Dimensions in m

flow is applied, as shown Fig. 22a. Figure 22b presents the streamlines of velocity field in the pipe-junction optimized for the turbulent flow.

Figure 23 presents the angled views including the finite element meshes of the pipe-junction optimized for turbulent flow from Fig. 21d. The advantages of decoupling the optimization and analysis meshes are highlighted here. In a fixed grid approach, this pipe-junction analysis would be tied to the 100×100×100 optimization mesh, which means a turbulent flow would be solved using at least 1,000,000 elements. Herein, by trimming out the design domain and meshing the remaining CAD geometry, the 3D pipe-junction from Fig. 23 is meshed with 69615 tetrahedral elements, a much lower amount if compared to the optimization mesh. This is especially advantageous for 3D as, besides employing a turbulence model with known accuracy, the computational time required is reduced. Herein, the FEA solver (forward and adjoint problems) took in average 2 minutes to run in each iteration of the 3D pipe-junction.

Figure 24 presents the streamlines of the fluid velocities flowing from both inlets, where the one flowing from inlet 1 is highlighted in blue color, and the one flowing from inlet 2 is highlighted with red color. Figure 24a shows the streamlines for the full design domain. It can be observed

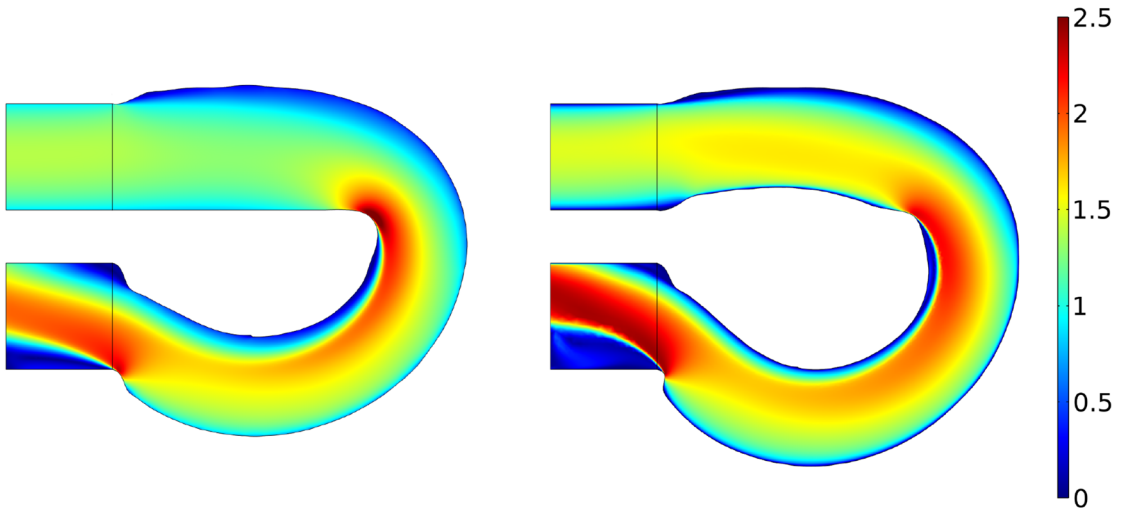


(a) $k$-$\varepsilon$; velocity (in m/s). (b) $k$-$\omega$; velocity (in m/s).

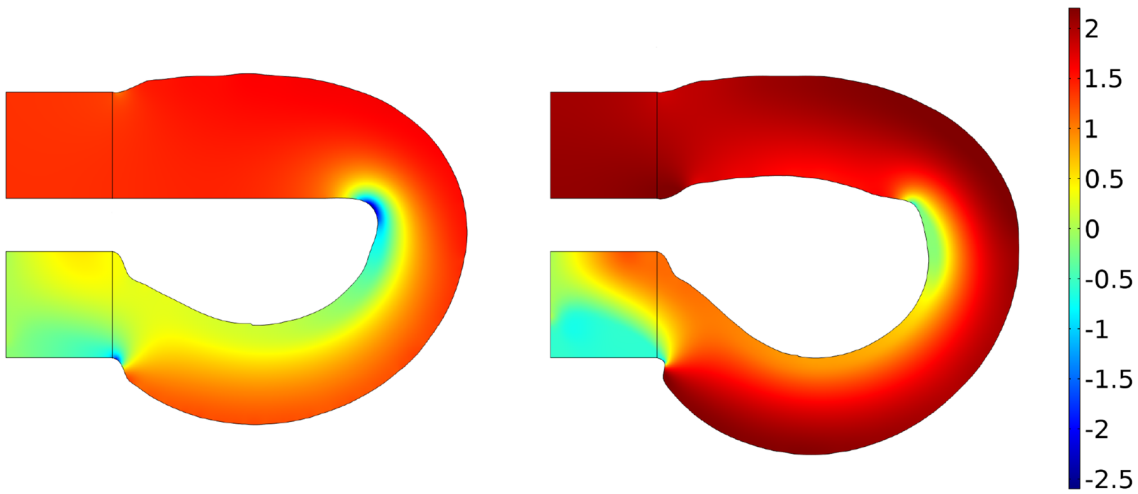


(c) $k$-$\varepsilon$; pressure (in Pa). (d) $k$-$\omega$; pressure (in Pa).

**Fig. 16** U-bend designs for Re = 5000 using the proposed TOBS-GT method: velocity fields (in m/s) when using the **a** $k$-$\varepsilon$ and **b** $k$-$\omega$ turbulence models and pressure fields (in Pa) when using the **c** $k$-$\varepsilon$ and **d** $k$-$\omega$ turbulence models

a large region of vortices and some mixing of the fluids coming from both inlets. Figure 24b presents the streamlines for the initial guess design. In this configuration, inlet 1 flow's inertia makes the fluid pass over the flow from inlet 2 and exit through the top half of the outlet cross-section. Meanwhile, the inlet 2 fluid flows under the inlet 1 flow and exits through the outlet's bottom half. The streamlines of the obtained optimized solution for Re = 5000 are shown in Fig. 24c. Similarly to the initial guess design case, the inlet 2 fluid flows under the inlet 1 flow, but no vortices are observed and the fluid flows much smoother than for the full design domain and the initial guess cases.

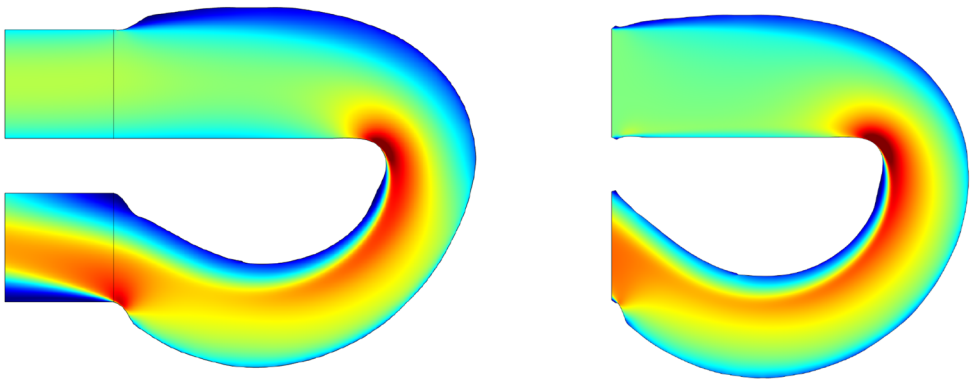

(a) Case with a smaller outlet tube and evaluation of the objective function including the inlet and outlet tubes.

(b) Case with neither inlet nor outlet tubes.

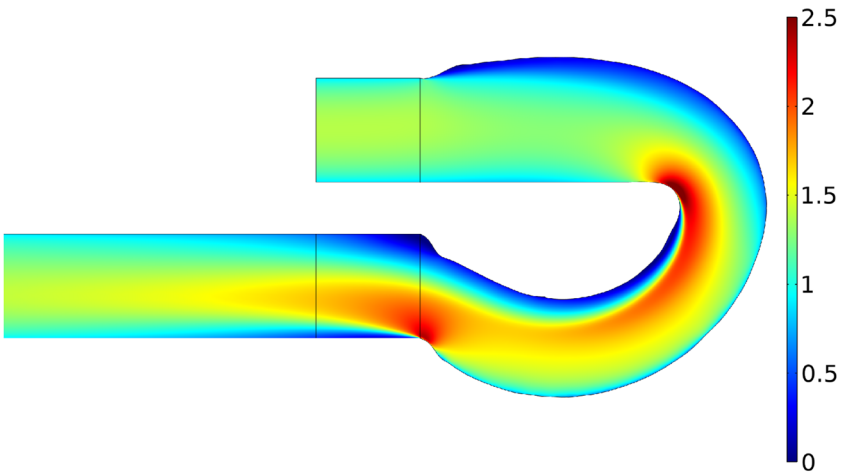


(c) Case with larger outlet tube.

**Fig. 17** U-bend solutions (velocity plot in m/s) using the $k$-$\varepsilon$ turbulence model for different inlet/outlet configurations. Dimensions in m

## 6 Conclusions

This paper presented a novel fluid flow topology optimization methodology based on the decoupling of the optimization variables and the finite element mesh. For that, the standard TOBS method (Sivapuram and Picelli 2018; Picelli et al. 2020b; Souza et al. 2021) is combined with a geometry trimming procedure to remove the solid regions from the fluid analysis domain, creating the so called TOBS-GT method. A filtering for extracting smooth contours is employed. One advantage is the possibility of obtaining smooth and explicitly defined fluid flow walls, particularly beneficial for turbulent flow problems with the inclusion of turbulence wall functions. Besides, the binary approach produces convergent solutions with no influence of the classic inverse permeability parameter. Therefore, the proposed methodology tackles the main three challenges in fluid flow topology optimization, i.e., the lack of explicit fluid walls during optimization, convergence to binary designs and the sometimes-exhausting parameters

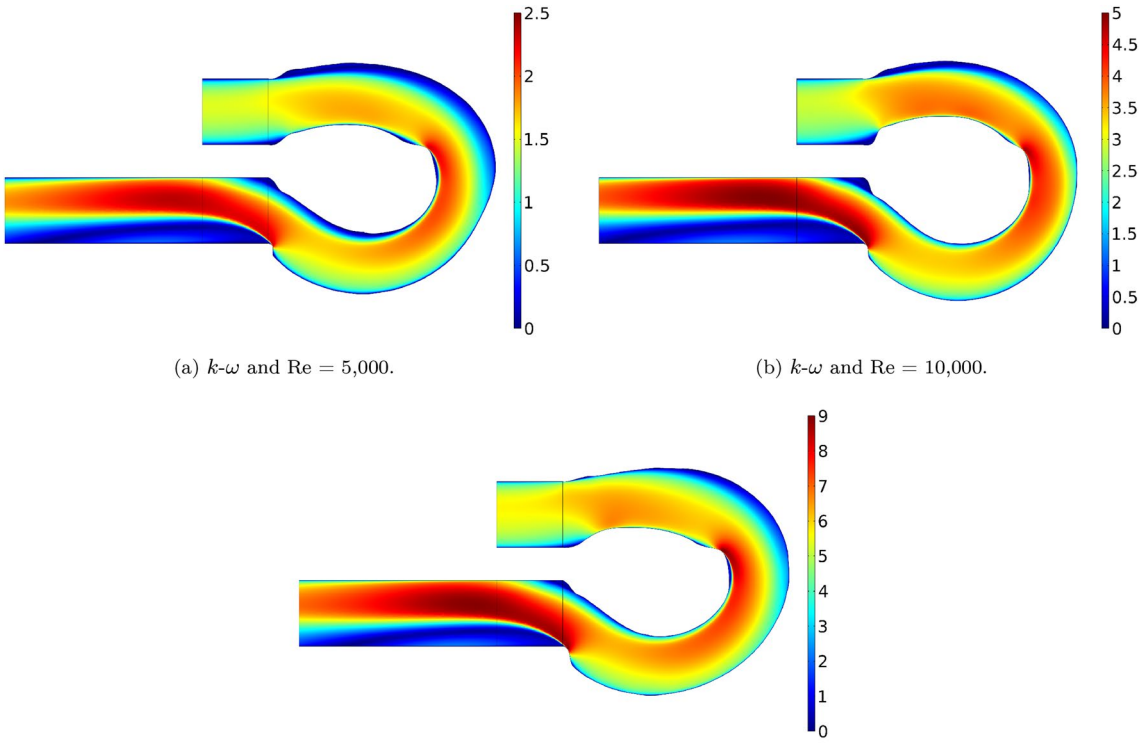


(a) $k$-$\omega$ and Re = 5,000. (b) $k$-$\omega$ and Re = 10,000.

(c) $k$-$\omega$ and Re = 20,000.

**Fig. 18** Velocity fields (in m/s) of the U-bend designs (larger outlet case) obtained with the proposed TOBS-GT method using the $k$-$\omega$ turbulent flow for **a** Re = 5000, **b** Re = 10,000 and **c** Re = 20,000

tuning. Numerical results show that the proposed TOBS-GT method tends to produce designs that are similar to those obtained with high inverse permeability values by the standard approach. The proposed binary framework favors combining the optimization with commercial FEA packages and automatic differentiation. It was also shown that the method can consider different governing equations, herein the $k$-$\varepsilon$ and $k$-$\omega$ turbulent flows. A cross-check analysis showed that the obtained designs are good optimized solutions if compared to solutions with enforced symmetry and baseline designs. Computational time studies show that the FEA is still the bottleneck of the optimization and that freely meshing only the fluid analysis domain can drastically reduce the amount of elements used in the simulation, especially for 3D problems.

## The sensitivity analysis

The present study adopts the adjoint sensitivity analysis via automatic differentiation to compute the sensitivity values of the fluid energy dissipation function. To verify the accuracy of this computation, the sensitivities of the pipe-bend example from Fig. 9 are compared to the finite difference method. The parameters and properties used are the same as for the pipe-bend example, except that $\kappa_{\max} = 10^6$ kg/(m$^3$ s) and Re = 2000. Fig. 25a presents the 100×100 finite element mesh used. In the current computational set up, the density variables are defined at the nodes of the mesh. All densities are defined as $\alpha = 1$. Figure 25b presents the volume-averaged adjoint sensitivity field computed via automatic differentiation, in

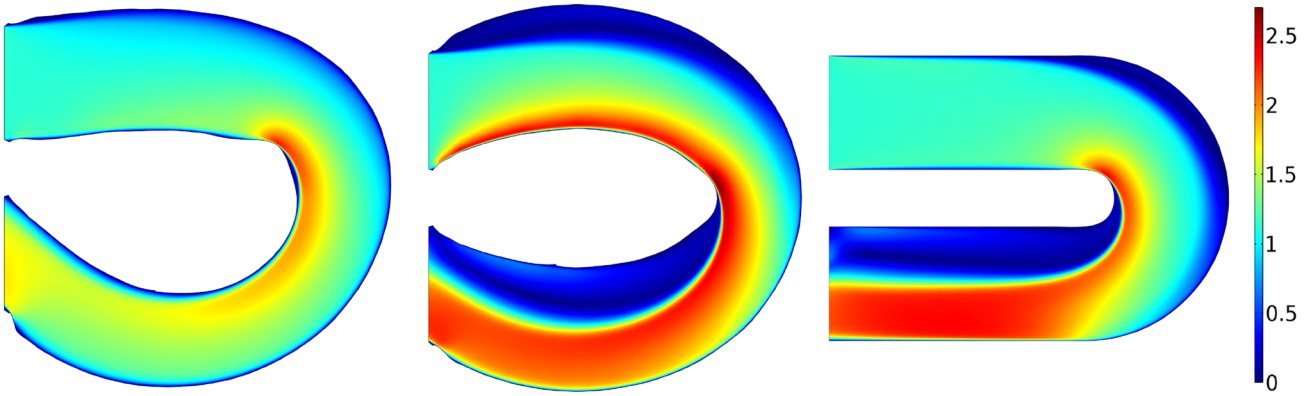


(a) TOBS-GT solution. Velocity field (m/s).

(b) TOBS-GT solution enforcing symmetry. Velocity field (m/s).

(c) Baseline solution. Velocity field (m/s).

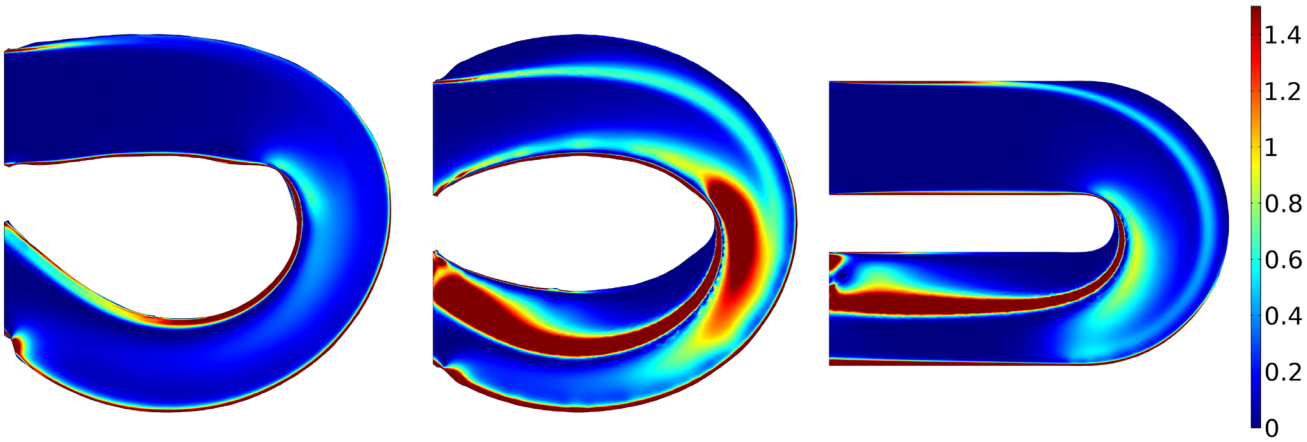


(d) Local energy dissipation; $\Phi = 6.47 \times 10^{-2}$ W/m.

(e) Local energy dissipation; $\Phi = 8.46 \times 10^{-2}$ W/m.

(f) Local energy dissipation; $\Phi = 9.25 \times 10^{-2}$ W/m.

**Fig. 19** Velocity fields, in m/s, and local energy dissipation $(\mu + \mu_T)(\nabla \boldsymbol{v} + (\nabla \boldsymbol{v})^T) \cdot (\nabla \boldsymbol{v} + (\nabla \boldsymbol{v})^T)$, in W/m, of the U-bend designs using the $k$-$\omega$ turbulent flow for Re = 5000 **a** and **d** obtained with the proposed TOBS-GT method, **b** and **e** solution with enforced symmetry and **c** and **f** baseline solution. The colorbar for local energy dissipation is clipped at 1.5 for better visualization

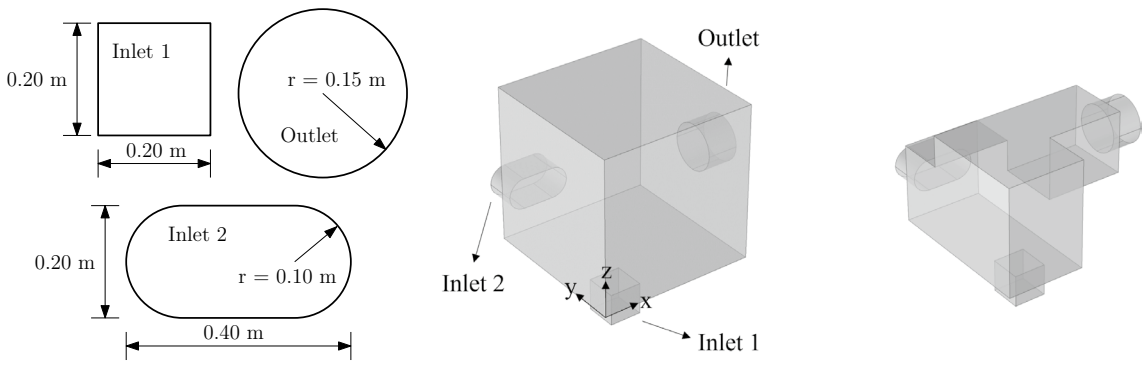


**(a)** Inlets and outlets. **(b)** Design domain of 1 m × 1 m × 1 m. **(c)** Initial guess design.

**Fig. 20** The 3D pipe-junction design problem: **a** inlets and outlet geometries, **b** design domain and **c** initial guess design

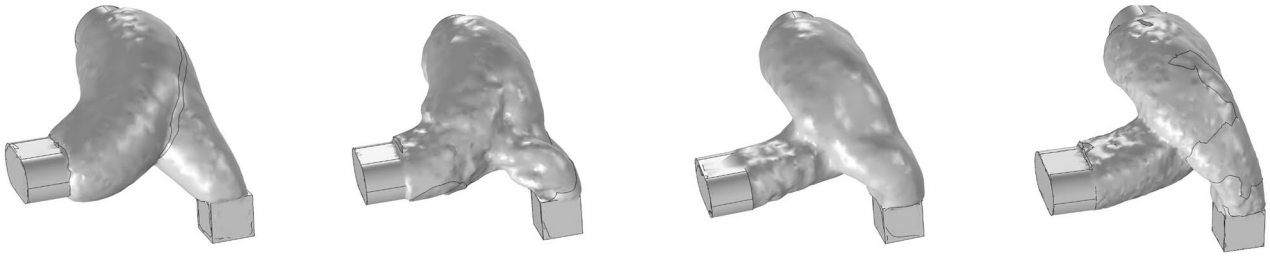

(a) Solution for Re = 0,001. (b) Re = 5,000, it. 4. (c) Re = 5,000, it. 8. (d) Re = 5,000, it. 12.

**Fig. 21** 3D pipe-junction optimized via the TOBS-GT method for **a** the laminar flow with Re = 0.001 and **b** iteration 4, **c** iteration 8 and **d** the final solution for the $k$-$\varepsilon$ turbulent flow with wall functions and Re = 5000

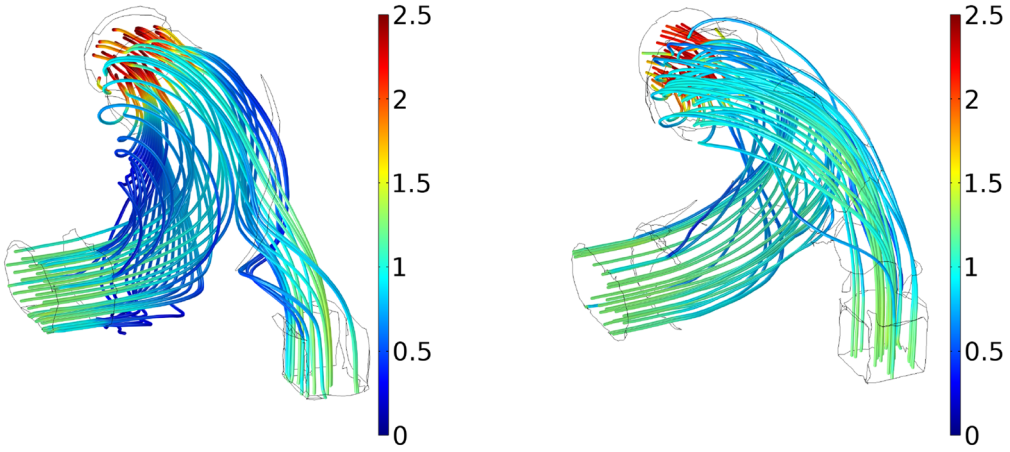


(a) Turbulent flow (Re = 5,000) in the design optimized for laminar flow, from Fig. 21a. (b) Turbulent flow (Re = 5,000) in the design optimized for turbulent flow, from Fig. 21d

**Fig. 22** Streamlines of the turbulent flow velocity field (in m/s) in the 3D pipe-junction optimized for **a** the laminar flow (Fig. 21a) and **b** the turbulent flow (Fig. 21d)

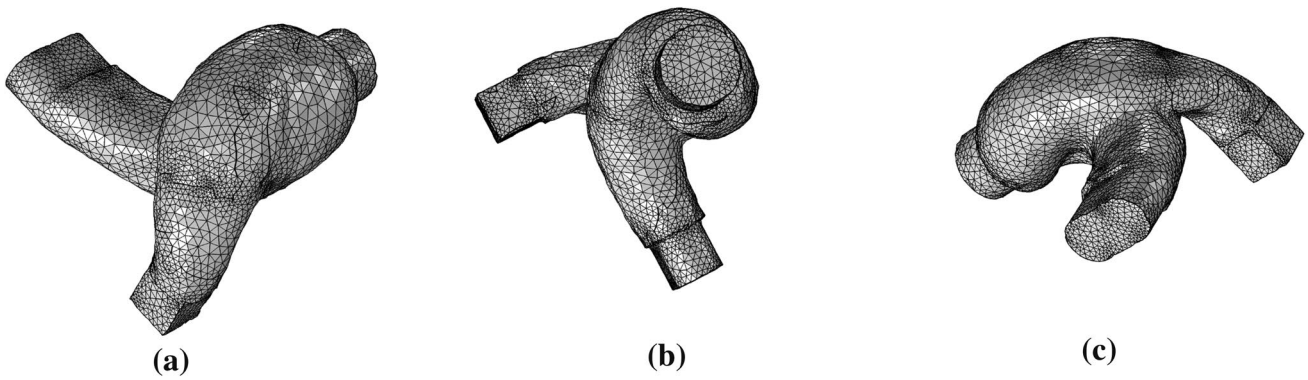


**Fig. 23** Angled views including the finite element meshes of the 3D pipe-junction optimized via the TOBS-GT method for the $k$-$\varepsilon$ turbulent flow with Re = 5000 and wall functions

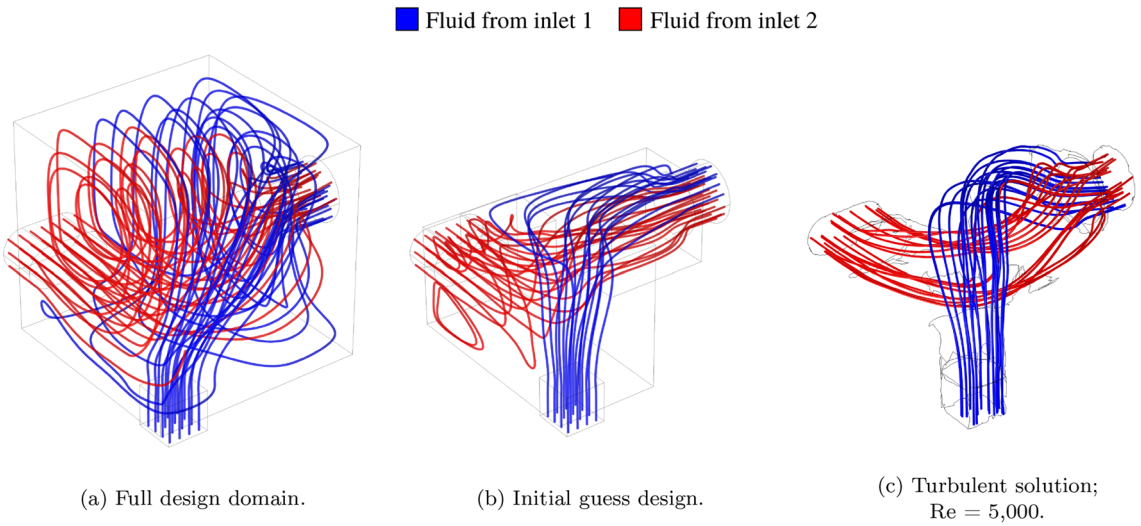


(a) Full design domain. (b) Initial guess design. (c) Turbulent solution; Re = 5,000.

**Fig. 24** Streamlines of the velocity field obtained with the $k$-$\varepsilon$ turbulent flow with wall functions and Re = 5000 for **a** the full design domain, **b** the initial guess design and **c** the optimized 3D pipe-junction by the TOBS-GT. The streamlines are plotted in blue for the fluid entering the inlet 1 and in red for the fluid entering the inlet 2. Both fluids have the same properties

**Table 1** Comparison between the obtained adjoint sensitivities against finite differences

| Coordinates $(x, y)$ in m | Perturbation | AD sensitivity | FD sensitivity | Error (%) |
|---|---|---|---|---|
| (0.7, 0.4) | $1\times10^{-4}$ | − 618521.69 | − 628516.04 | 1.5902 |
| (0.8, 0.3) | $1\times10^{-4}$ | − 618143.65 | − 628866.34 | 1.7051 |
| (0.6, 0.5) | $1\times10^{-4}$ | − 624916.01 | − 612625.54 | 2.0062 |
| (0.1, 0.7) | $1\times10^{-4}$ | − 217548.12 | − 218794.15 | 0.5695 |
| (0.5, 0.7) | $1\times10^{-4}$ | − 282819.64 | − 284408.03 | 0.4960 |
| (0.0, 0.8) | $1\times10^{-4}$ | − 583161.94 | − 554313.66 | 5.2043 |
| (0.1, 0.1) | $1\times10^{-5}$ | 15605.33 | 15212.69 | 2.581 |
| (0.7, 0.2) | $1\times10^{-6}$ | − 167300.62 | − 173446.05 | 3.5431 |
| (0.1, 1.0) | $1\times10^{-6}$ | 7138.61 | 7068.24 | 0.99559 |
| (0.8, 0.0) | $1\times10^{-6}$ | − 600988.69 | − 596612.45 | 0.7335 |

1/m$^2$. Figure 25c presents the local fluid energy dissipation $(\mu + \mu_T)(\nabla \boldsymbol{v} + (\nabla \boldsymbol{v})^T) \cdot (\nabla \boldsymbol{v} + (\nabla \boldsymbol{v})^T)$, in W/m, clipped at 1 for better visualization. Some points inside low and high dissipation regions are chosen to compare the sensitivities against finite differences. These points, the perturbation, the computed sensitivities via the adjoint (AD) and the finite difference (FD) method and the relative errors are presented in Table 1. The errors showed to be between 0.5% and 8.5%. Eventually, some of the errors might be caused by some terms that are ignored in the computation of the Jacobian matrix for the adjoint problem, so-called "nojac" terms by the automatic differentiation module used. Otherwise, the tolerance on the residual of the governing equations by the FEA solver can also increase the error. Anyway, in general, the sensitivities showed throughout this work to provide good directions

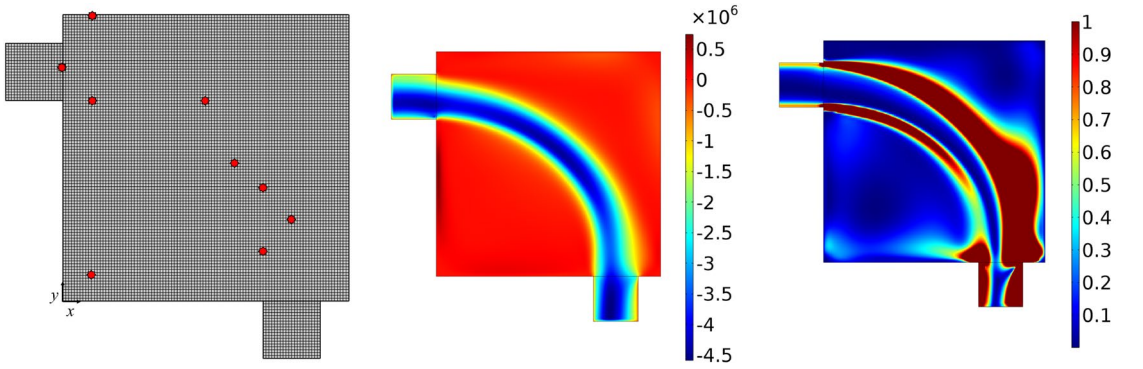


(a) Points and finite element mesh. (b) Adjoint sensitivities (1/m$^2$). (c) Local fluid energy dissipation (W/m).

**Fig. 25** Sensitivity analysis of the pipe-bend example

to minimize the objective function, verified by some cross-check analyses.

**Funding information** This research was partly supported by CNPq (Brazilian Research Council) and FAPESP (São Paulo Research Foundation). The authors thank the supporting institutions. The first author thanks FAPESP under the Young Investigators Awards program, grants 2018/05797-8 and 2019/01685-3. The first and second authors thank FUSP (University of São Paulo Foundation), project numbers 314139 and 314137. The fourth author thanks FAPESP under grant 2017/27049-0. The last author thanks the financial support of CNPq (National Council for Research and Development) under grant 302658/2018-1 and FAPESP under grant 2013/24434-0. The authors also acknowledge the support of the RCGI (Research Centre for Gas Innovation), hosted by the University of São Paulo (USP) and sponsored by FAPESP (2014/50279-4) and Shell Brazil.

## Declarations

**Conflict of interest** The authors declare that they have no conflict of interest.

**Replication of results** The results presented in this work can be reproduced by following the algorithms and formulations presented in detail herein. The TOBS implementation is presented in www.github.com/renatopicelli/tobs and in Picelli et al. (2020b).

## References

Alexandersen J, Andreasen CS (2020) A review of topology optimisation for fluid-based problems. Fluids 5(5):29

Alonso DH, de Sá LFN, Saenz JSR, Silva ECN (2018) Topology optimization applied to the design of 2d swirl flow devices. Struct Multidisc Optim 58(6):2341–2364. https://doi.org/10.1007/s00158-018-2078-0

Andreasen CS, Gersborg AR, Sigmund O (2009) Topology optimization of microfluidic mixers. Int J Numer Meth Fluids 61:498–513. https://doi.org/10.1002/fld.1964

Borrvall T, Petersson J (2003) Topology optimization of fluids in Stokes flow. Int J Numer Meth Fluids 41:77–107

Brinkman HC (1947) A calculation of the viscous force exerted by a flowing fluid on a dense swarm of particles. J Appl Sci Res A1:27–34

COMSOL (2019) COMSOL multiphysics reference manual, version 5.5, COMSOL, Inc. COMSOL

Dilgen CB, Dilgen SB, Fuhrman DR, Sigmund O, Lazarov BS (2018) Topology optimization of turbulent flows. Comput Methods Appl Mech Eng 331:363–393. https://doi.org/10.1016/j.cma.2017.11.029

Dilgen SB, Dilgen CB, Fuhrman DR, Sigmund O, Lazarov BS (2018) Density based topology optimization of turbulent flow heat transfer systems. Struct Multidisc Optim 57:1905–1918. https://doi.org/10.1007/s00158-018-1967-6

Feppon F, Allaire G, Bordeu F, Cortial J, Dapogny C (2019) Shape optimization of a coupled thermal fluid-structure problem in a level set mesh evolution framework. SeMA J 76(3):413–458

Gersborg-Hansen A, Bendsøoe MP, Sigmund O (2006) Topology optimization of heat conduction problems using the finite volume method. Struct Multidisc Optim 31(4):251–259

Haftka RT, Gürdal Z (1992) Elements of structural optimization. Kluwer Academic Publishers, Dordrecht

Hyun J, Wang S, Yang S (2014) Topology optimization of the shear thinning non-Newtonian fluidic systems for minimizing wall shear stress. Comput Math Appl 67(5):1154–1170. https://doi.org/10.1016/j.camwa.2013.12.013

Jensen KE, Szabo P, Okkels F (2012) Topology optimization of viscoelastic rectifiers. Appl Phys Lett 100(23):234102:1-234102:3

Kontoleontos EA, Papoutsis-Kiachagias EM, Zymaris AS, Papadimitriou DI, Giannakoglou KC (2013) Adjoint-based constrained topology optimization for viscous flows, including heat transfer. Eng Optim 45(8):941–961

Kubo S, Koguchi A, Yaji K, Yamada T, Izui K, Nishiwaki S (2021) Level set-based topology optimization for two dimensional turbulent flow using an immersed boundary method. J Comput Phys 446:110630

Land AH, Doig AG (1960) An automatic method of solving discrete programming problems. Econometrica 28:497–520

Larsson J (1998) Numerical Simulation of Turbulent Flows for Turbine Blade Heat Transfer. PhD thesis, Chalmers University of Technology, Sweden

Lee JS, Ha MY, Min JK (2020) A finite-volume based topology optimization procedure for an aero-thermal system with a simplified sensitivity analysis method. Int J Heat Mass Transf 163:120524

Othmer C (2008) A continuous adjoint formulation for the computation of topological and surface sensitivities of ducted ows. Int J Numer Meth Fluids 58:861–877

Papoutsis-Kiachagias Giannakoglou KC (2016) Continuous adjoint methods for turbulent flows, applied to shape and topology optimization: industrial applications. Arch Comput Methods Eng 23:255–299

Paul WH (2009) Logic and integer programming, international series in operations research and management science, vol 130, 1st edn. Springer, New York. https://doi.org/10.1007/978-0-387-92280-5

Picelli R, Ranjbarzadeh S, Sivapuram R, Gioria RS, Silva ECN (2020) Topology optimization of binary structures under design-dependent fluid-structure interaction loads. Struct Multidisc Optim 62:2101–2116

Picelli R, Sivapuram R, Xie YM (2020) A 101-line MATLAB code for topology optimization using binary variables and integer programming. Struct Multidisc Optim 63:935–954

Pingen G, Maute K (2010) Optimal design for non-Newtonian flows using a topology optimization approach. Comput Math Appl 59(7):2340–2350

Pizzolato A (2018) Topology optimization for energy problems. PhD thesis, Politecnico di Torino

Romero JS, Silva ECN (2014) A topology optimization approach applied to laminar flow machine rotor design. Comput Methods Appl Mech Eng 279:268–300. https://doi.org/10.1016/j.cma.2014.06.029

Sá LF, Romero JS, Horikawa O, Silva ECN (2018) Topology optimization applied to the development of small scale pump. Struct Multidisc Optim 57(5):2045–2059. https://doi.org/10.1007/s00158-018-1966-7

Savitzky A, Golay MJE (1964) Smoothing and differentiation of data by simplified Least Squares procedures. Anal Chem 36:1627–1639

Sivapuram R, Picelli R (2018) Topology optimization of binary structures using Integer Linear Programming. Finite Elem Anal Des 139:49–61

Sivapuram R, Picelli R (2020) Topology design of binary structures subjected to design-dependent thermal expansion and fluid pressure loads. Struct Multidisc Optim 61:1877–1895

Sivapuram R, Picelli R, Xie YM (2018) Topology optimization of binary microstructures involving various non-volume constraints. Comput Mater Sci 154:405–425

Song XG, Wang L, Baek SH, Park YC (2009) Multidisciplinary optimization of a butterfly valve. ISA Trans 48(3):370–377

Souza BC, Yamabe PVM, Sá LFN, Ranjbarzadeh S, Picelli R, Silva ECN (2021) Topology optimization of fluid flow by using integer linear programming. Struct Multidisc Optim 64:1221–1240

Sá LFN, Yamabe PVM, Souza BC, Silva ECN (2021) Topology optimization of turbulent rotating flows using Spalart–Allmaras model. Comput Methods Appl Mech Eng 373:113551

Vanderbei RJ (2014) Linear programming: foundations and extensions, 4th edn. Springer, New York

Wilcox DC (1998) Turbulence modeling for CFD, 2nd edn. DCW Industries, New York

Wilcox DC (2008) Formulation of the k-omega turbulence model revisited. AIAA J 46(11):2823–2838

Yoon GH (2016) Topology optimization for turbulent flow with Spalart–Allmaras model. Comput Methods Appl Mech Eng 303:288–311. https://doi.org/10.1016/j.cma.2016.01.014

Yoon GH (2020) Topology optimization method with finite elements based on the k--ε turbulence model. Comput Methods Appl Mech Eng 361:112784. https://doi.org/10.1016/j.cma.2019.112784